LETTER

https://doi.org/10.1038/s41586-019-0916-x

Anti–tumour immunity controlled through mRNA m^6A methylation and YTHDF1 in dendritic cells

Dali Han[1,2,3,11,12]*, Jun Liu[4,5,6,11], Chuanyuan Chen[1,2,3], Lihui Dong[7], Yi Liu[7], Renbao Chang[1,2], Xiaona Huang[8], Yuanyuan Liu[9], Jianying Wang[9], Urszula Dougherty[10], Marc B. Bissonnette[10], Bin Shen[9], Ralph R. Weichselbaum[8], Meng Michelle Xu[7,12]* & Chuan He[4,5,6,12]*

There is growing evidence that tumour neoantigens have important roles in generating spontaneous antitumour immune responses and predicting clinical responses to immunotherapies[1,2]. Despite the presence of numerous neoantigens in patients, complete tumour elimination is rare, owing to failures in mounting a sufficient and lasting antitumour immune response[3,4]. Here we show that durable neoantigen-specific immunity is regulated by mRNA N^6-methyadenosine (m^6A) methylation through the m^6A-binding protein YTHDF1[5]. In contrast to wild-type mice, *Ythdf1*-deficient mice show an elevated antigen-specific $CD8^+$ T cell antitumour response. Loss of YTHDF1 in classical dendritic cells enhanced the cross-presentation of tumour antigens and the cross-priming of $CD8^+$ T cells in vivo. Mechanistically, transcripts encoding lysosomal proteases are marked by m^6A and recognized by YTHDF1. Binding of YTHDF1 to these transcripts increases the translation of lysosomal cathepsins in dendritic cells, and inhibition of cathepsins markedly enhances cross-presentation of wild-type dendritic cells. Furthermore, the therapeutic efficacy of PD-L1 checkpoint blockade is enhanced in *Ythdf1*$^{-/-}$ mice, implicating YTHDF1 as a potential therapeutic target in anticancer immunotherapy.

Spontaneous priming of T cells against tumour neoantigens is crucial for the clinical efficacy of immunotherapies. However, in many patients, neoantigen recognition is insufficient to induce the lasting T cell response that is required for complete tumour rejection. The identification of molecular pathways that influence immunoreactivity to tumour neoantigens could provide new targets for improving the response to immunotherapy.

m^6A, the most abundant internal mRNA modification, is responsible for the post-transcriptional regulation of mRNA in diverse cell types[6–10]. m^6A can affect the efficiency of mRNA translation via the m^6A-binding protein YTHDF1[5]. Dysregulation of m^6A pathway components could affect oncogene expression, thereby linking m^6A and tumorigenesis[11–14]. As most studies focus on tumour-intrinsic oncogenic pathways, potential roles of the mRNA m^6A modification in host antitumour immune responses are unknown. Furthermore, the roles of various m^6A reader proteins in cancer have been largely unexplored.

We inoculated ovalbumin (OVA)-expressing B16 melanoma cells subcutaneously into wild-type and *Ythdf1*$^{-/-}$ mice[15] (Extended Data Fig. 1). Compared to wild-type mice, *Ythdf1*$^{-/-}$ mice showed slower growth of B16-OVA tumours and prolonged survival (Fig. 1a, Extended Data Fig. 2a, b). We also tested the MC38 colon carcinoma model, which has been reported to have a broader neoantigen pool[16]. Consistently, we observed a similar level of tumour inhibition in *Ythdf1*$^{-/-}$ and wild-type mice (Fig. 1b, Extended Data Fig. 2c). Immune infiltrates contained higher levels of $CD8^+$ cytotoxic T cells and natural killer (NK) cells in tumours from *Ythdf1*$^{-/-}$ mice than from wild-type mice, suggesting that immunosurveillance is enhanced in the absence of YTHDF1 (Fig. 1c). Accordingly, we observed reduced infiltration of myeloid-derived suppressor cells (MDSCs) in tumours from *Ythdf1*$^{-/-}$mice (Extended Data Fig. 2d, e), whereas there was no significant difference in the number of T regulatory (T_{reg}) cells (Extended Data Fig. 2f, g). Both $CD8^+$ T cells and NK cells are critical for controlling tumour growth[17], so we dissected their contributions to the anti-tumour response in *Ythdf1*$^{-/-}$mice. NK cells from wild-type and *Ythdf1*$^{-/-}$ mice showed similar degranulation responses (Extended Data Fig. 2h), and antibody-mediated depletion of NK cells had no effect on tumour growth in *Ythdf1*$^{-/-}$ mice (Fig. 1d, Extended Data Fig. 2i). By contrast, the anti-tumour response in *Ythdf1*$^{-/-}$ mice was completely abrogated in the absence of $CD8^+$ T cells (Fig. 1e, Extended Data Fig. 2i), indicating that $CD8^+$ T cells are essential for tumour control in the *Ythdf1*-deficient host.

To determine whether neoantigen-specific $CD8^+$ T cell responses are generated in B16-OVA tumours, we analysed the frequency of tumour-infiltrating $CD8^+$ T cells expressing the SIINFEKL MHC-I tetramer in wild-type and *Ythdf1*$^{-/-}$ mice. Whereas wild-type mice did not accumulate antigen-specific $CD8^+$ T cells within the tumour, *Ythdf1*$^{-/-}$ mice showed a substantial increase in $CD8^+$ T cells against tumour neoantigen in vivo (Fig. 2a, b). To investigate whether the infiltration of neoantigen-specific $CD8^+$ T cells in *Ythdf1*$^{-/-}$ mice was due to enhanced spontaneous $CD8^+$ T cell priming at an early stage, we stimulated lymphocytes from tumour-draining lymph nodes (DLNs) in vitro with or without OVA-derived SIINFEKL peptide or tumour cells, and measured endogenous $CD8^+$ T cell responses using enzyme-linked immune absorbent spot (ELISPOT) testing for interferon-γ (IFNγ). There were substantially more IFNγ spot-forming cells in *Ythdf1*$^{-/-}$ mice than in wild-type mice in both B16-OVA and MC38 tumour models (Fig. 2c, d), indicating that YTHDF1 depletion in host cells potentiates the early steps of T cell priming against tumour neoantigens.

Next, we showed that loss of *Ythdf1* in T cells makes a minor contribution to the observed antitumour immunity (Extended Data Fig. 3a). As dendritic cells (DCs) are the main antigen-presenting cells (APCs) that cross-prime $CD8^+$ T cells, we hypothesized that the increased T cell priming in *Ythdf1*$^{-/-}$ mice could be attributed to improved recognition of tumour cells through an increased cross-priming ability of DCs[18,19]. To test this hypothesis, we used classical DCs cultured in medium supplemented with FLT3L (FLT3L-DCs) to model how cross-presentation occurs[20–22]. We pulsed FLT3L-DCs with necrotic B16-OVA in vitro

[1]Key Laboratory of Genomic and Precision Medicine, Beijing Institute of Genomics, Chinese Academy of Sciences, Beijing, China. [2]Institute for Stem Cell and Regeneration, Chinese Academy of Sciences, Beijing, China. [3]College of Future Technology, Sino-Danish College, University of Chinese Academy of Sciences, Beijing, China. [4]Department of Chemistry, The University of Chicago, Chicago, IL, USA. [5]Department of Biochemistry and Molecular Biology, The University of Chicago, Chicago, IL, USA. [6]Institute for Biophysical Dynamics, Howard Hughes Medical Institute, The University of Chicago, Chicago, IL, USA. [7]Department of Basic Medical Sciences, School of Medicine, Institute for Immunology, Beijing Key Lab for Immunological Research on Chronic Diseases, THU-PKU Center for Life Sciences, Tsinghua University, Beijing, China. [8]Department of Radiation and Cellular Oncology, The Ludwig Center for Metastasis Research, University of Chicago, Chicago, IL, USA. [9]State Key Laboratory of Reproductive Medicine, Department of Histology and Embryology, Nanjing Medical University, Nanjing, China. [10]Department of Medicine, The University of Chicago, Chicago, IL, USA. [11]These authors contributed equally: Dali Han, Jun Liu. [12]These authors jointly supervised this work: Dali Han, Meng Michelle Xu, Chuan He. *e-mail: handl@big.ac.cn; michellexu@mail.tsinghua.edu.cn; chuanhe@uchicago.edu

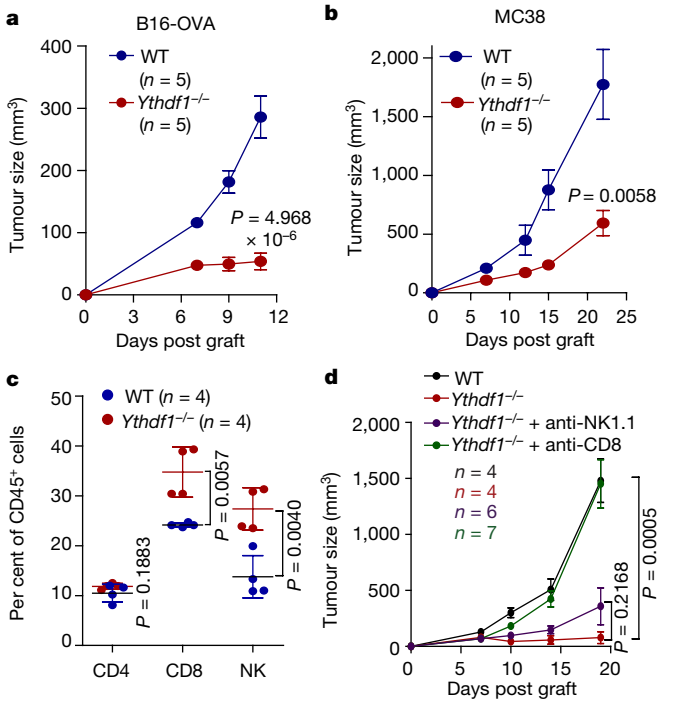

Fig. 1 | *Ythdf1*$^{-/-}$ mice show effective tumour control that depends on CD8$^+$ T cells. a, Wild-type or *Ythdf1*$^{-/-}$ mice were injected subcutaneously with 10^6 B16-OVA cells. Tumour growth was monitored. One of three representative experiments is shown. **b**, Wild-type or *Ythdf1*$^{-/-}$ mice were injected subcutaneously with 10^6 MC38 cells. Tumour growth was monitored. One of three representative experiments is shown. **c**, Percentage of tumour-infiltrating T cells and NK cells on day 12 post tumour inoculation. **d**, Wild-type and *Ythdf1*$^{-/-}$ mice were injected subcutaneously with 10^6 B16-OVA cells and treated with 200 μg of CD8- or NK-depleting antibody twice a week starting on day 3. Tumour size was monitored over time. *n*, number of mice. Mean ± s.e.m., two-sided unpaired Student's *t*-test.

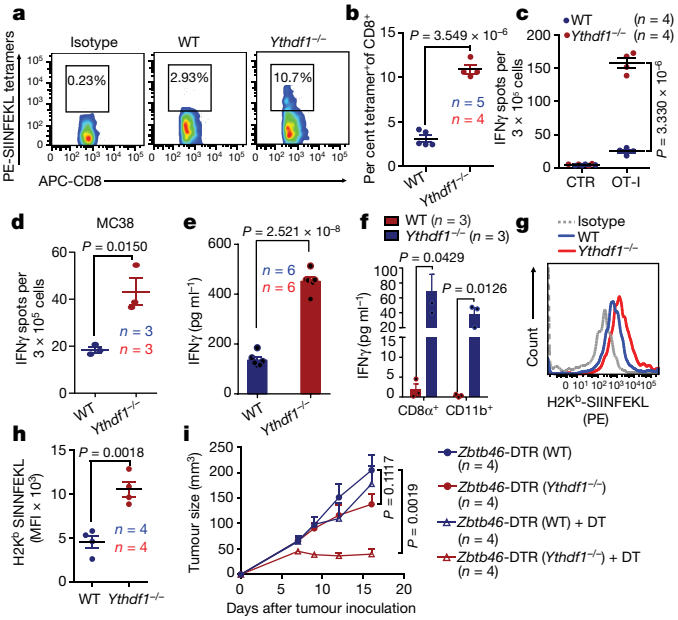

Fig. 2 | Cross-priming capacity of DCs is enhanced in *Ythdf1*$^{-/-}$ mice. a–**c**, Wild-type or *Ythdf1*$^{-/-}$ mice were injected subcutaneously with 10^6 B16-OVA cells. The frequency of tumour-infiltrating OVA-specific CD8$^+$ T cells was assessed 12 days after tumour inoculation (**a**, **b**). Six days after tumour inoculation, lymphocytes from DLNs were isolated and stimulated with 1 μg ml$^-$ OTI peptide. IFNγ-producing cells were enumerated by ELISPOT assay (**c**). **d**, Wild-type or *Ythdf1*$^{-/-}$ mice were injected subcutaneously with 10^6 MC38 cells. Six days after tumour inoculation, lymphocytes from DLNs were isolated and stimulated with irradiated MC38 cells for 48 h. IFNγ-producing cells were enumerated by ELISPOT assay. **e**, FLT3L-DCs were co-cultured with necrotic B16-OVA overnight, and CD11c$^+$ cells were purified and co-cultured with OT-I T cells. IFNγ production was assessed by IFNγ cytometric bead array. Data are representative of six biological replicates. **f**, Six days after tumour inoculation, CD8$^+$ or CD11b$^+$ DCs were sorted from DLNs. DCs were co-cultured with isolated OT-I cells for 3 days and analysed by IFNγ cytometric bead assay (CBA). **g**, **h**, Formation of H-2K^b-SIINFEKL on tumour-infiltrating DCs from B16-OVA tumour-bearing wild-type and *Ythdf1*$^{-/-}$ mice (**g**). Mean fluorescence intensity (MFI) is shown (**h**). **i**, Wild-type mice were injected with wild-type or *Ythdf1*$^{-/-}$ BMCs mixed with *Zbtb46*-DTR BMCs in a 1:1 ratio. Six weeks after bone marrow chimaera reconstitution, mice were injected subcutaneously with 1×10^6 B16-OVA cells. Diphtheria toxin (400 ng) was administered on the same day (+ DT). Tumour size was monitored over time. *n*, number of mice. Mean ± s.e.m., two-sided unpaired Student's *t*-test. Data are representative of two independent experiments (**a**, **g**).

and evaluated their ability to cross-prime T cells expressing transgenic ovalbumin-specific (OT-I) T cell receptors. *Ythdf1*$^{-/-}$ FLT3L-DCs were able to cross-prime OT-I T cells to a greater extent than wild-type DCs (Fig. 2e). To determine the cross-priming capacity of classical DCs (cDCs) in vivo, we collected CD8α$^+$ DCs and CD11b$^+$ DCs from DLNs of B16-OVA- or MC38-OTIp-tumour bearing mice and co-cultured them with OT-I T cells. Whereas wild-type mice showed weak cross-priming of CD8$^+$ T cells, we observed substantially augmented T cell cross-priming induced by both CD8α$^+$ DCs and CD11b$^+$ DCs in *Ythdf1*$^{-/-}$ mice (Fig. 2f, Extended Data Fig. 3b). In addition, *Ythdf1*$^{-/-}$ DCs showed enhanced cross-presentation for the less sensitive model antigen SIY (Extended Data Fig. 3c). To test whether cross-priming in DCs depends on RNA m^{6}A methylation in general, we compared the cross-presentation capacity of *Mettl14*-deficient DCs from CD11c-Cre*Mettl14*$^{f/f}$ conditional knockout mice and wild-type DCs. DCs deficient in *Mettl14* showed enhanced cross-presentation ability (Extended Data Fig. 3d), confirming the critical role of the m^{6}A-YTHDF1 axis in restricting the cross-priming capacity of DCs.

To investigate whether the increased cross-capacity of YTHDF1-deficient DCs for priming could be attributed to differential expression of co-stimulatory molecules[23], we evaluated the expression of CD80 and CD86 on DCs. Wild-type and *Ythdf1*$^{-/-}$ DCs expressed comparable levels of CD80 and CD86, and also exhibited a similar ability to directly prime OT-I T cells with peptide stimulation (Extended Data Fig. 3e, f). In addition, loss of YTHDF1 did not affect the composition of DC subpopulations in naive mice (Extended Data Fig. 4), nor did it affect LPS-mediated activation of DCs (Extended Data Fig. 5a). These findings suggest that loss of YTHDF1 increases the cross-priming capacity of DCs, rather than affecting the development or activation of DCs.

To determine whether YTHDF1 deficiency enhances the cross-presentation of tumour antigens on DCs, leading to better cross-priming of CD8$^+$ T cells[24,25], we assessed the abundance of H-2K^b-SIINFEKL complexes on DCs from wild-type and *Ythdf1*$^{-/-}$ mice bearing B16-OVA tumours. Although phagocytosis of tumour cells was similar in wild-type and *Ythdf1*$^{-/-}$ mice (Extended Data Fig. 5b, c), the level of H-2K^b-SIINFEKL complexes was markedly higher in tumour-infiltrating *Ythdf1*$^{-/-}$ DCs than in wild-type DCs (Fig. 2g, h). Furthermore, compared with splenic wild-type DCs, DCs from *Ythdf1*$^{-/-}$ mice exhibited a higher potential for cross-presentation of soluble OVA in vitro (Extended Data Fig. 5d). These data suggest that DCs from *Ythdf1*$^{-/-}$ mice possess improved antigen-presentation relative to DCs from wild-type mice.

To investigate whether the antitumour immunity relies on loss of *Ythdf1* specifically in DCs, we generated chimeric, DC-specific *Ythdf1* knockout mice. Specifically, we reconstituted irradiated mice with a 1:1 mixture of *Ythdf1*$^{-/-}$ bone marrow cells (BMCs) and wild-type BMCs with a *Zbtb46*-DTR transgene, which drives expression of the diphtheria toxin receptor in classical DCs. Upon administration of diphtheria

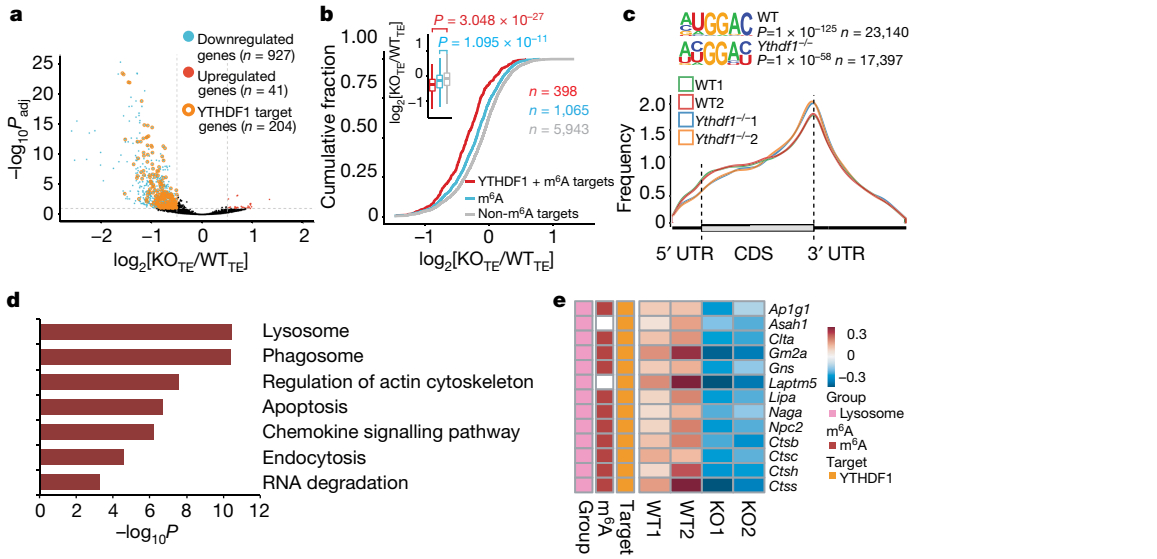

Fig. 3 | Transcriptome-wide identification and analysis of YTHDF1-binding sites. a, Volcano plots of genes with differential translational efficiency in wild-type and *Ythdf1*$^{-/-}$ FLT3L-DCs (adjusted $P \leq 0.1$ and fold change ≥ 0.5). Transcripts with YTHDF1-binding sites in 3′ UTR are shown with yellow circles. *P* values calculated with two-sided likelihood ratio test and adjusted by Benjamini–Hochberg method; $n = 4$ (2 conditions × 2 biological replicates). **b**, Cumulative distribution of the fold change in translational efficiency between wild-type (WT_{TE}) and *Ythdf1*$^{-/-}$ (KO_{TE}) FLT3L-DCs. *P* values calculated using two-sided Kolmogorov–Smirnov test; $n = 2$ independent biological replicates. Box-plot elements: centre line, median; box limits, upper and lower quartiles; whiskers, 1–99%. **c**, Metagene plot depicting nearly unchanged m^{6}A peak distribution and similar consensus motifs in wild-type (WT1 and WT2 represent replicates) and *Ythdf1*$^{-/-}$ (*Ythfd1*$^{-/-}$1 and *Ythfd1*$^{-/-}$2 represent replicates) FLT3L-DCs. *P* values of consensus motifs generated by HOMER[29] using one-sided binomial test. **d**, KEGG enrichment analysis of genes with significantly decreased translation efficiency (adjusted $P \leq 0.1$ and fold change ≤ -0.5) and YTHDF1-binding sites in 3′ UTR ($n = 204$). One-sided hypergeometric test was used to determine statistical significance of enrichment. **e**, Heatmap showing the translational efficiency of lysosome genes in wild-type and *Ythdf1*$^{-/-}$ (KO1 and KO2 represent replicates) FLT3L-DCs. *n*, number of genes or m^{6}A peaks.

toxin, wild-type cDCs expressing *Zbtb46*-DTR are selectively eliminated, with all remaining cDCs in *Zbtb46*-DTR:*Ythdf1*$^{-/-}$ mice being *Ythdf1*-deficient. We also established chimeric *Zbtb46*-DTR:*Ythdf1*$^{+/+}$ mice as controls. We found that B16-OVA tumours grew similarly in *Zbtb46*-DTR:*Ythdf1*$^{+/+}$ and *Zbtb46*-DTR:*Ythdf1*$^{-/-}$ chimeric mice that were not treated with diphtheria toxin (Fig. 2i). Notably, treatment with diphtheria toxin substantially reduced tumour growth in *Zbtb46*-DTR:*Ythdf1*$^{-/-}$ mice compared with *Zbtb46*-DTR:*Ythdf1*$^{+/+}$ mice (Fig. 2i). These data demonstrate that specific *Ythdf1* depletion in cDCs is sufficient to generate the antitumour response. Together, these findings suggest that YTHDF1 in cDCs limits their cross-presentation capacity in vivo, and that altered T cell or DC homeostasis or development in *Ythdf1*$^{-/-}$ mice does not contribute substantially to antitumour activity.

We next performed RNA immunoprecipitation and sequencing (RIP–seq) to map target transcripts bound by YTHDF1 in FLT3L-DCs. YTHDF1-binding sites were highly reproducible between two biological replicates (Extended Data Fig. 6a, b), and were predominantly distributed in the coding region and 3′ untranslated region (UTR; Extended Data Fig. 6c, d). Given that YTHDF1 is known to affect mRNA translation[5], we assessed the translational efficiency of wild-type and *Ythdf1*$^{-/-}$ DCs by ribosome profiling. We also performed antibody-based m^{6}A profiling and RNA sequencing (RNA-seq) in the same cells. We categorized transcripts into three groups: non-m^{6}A marked transcripts, m^{6}A-containing transcripts, and m^{6}A-marked transcripts bound by YTHDF1. As expected, we found a notable decrease in translation efficiency, particularly for YTHDF1-targeted and m^{6}A-marked transcripts, in *Ythdf1*$^{-/-}$ DCs compared with wild-type DCs (Fig. 3a, b), whereas *Ythdf1* deficiency did not substantially alter the distribution of m^{6}A in mRNAs from DCs (Fig. 3c).

To identify the functional pathways that are associated with YTHDF1-targeted mRNAs, we analysed m^{6}A-marked mRNAs that are both targets of YTHDF1 and translationally regulated by YTHDF1. We performed Kyoto Encyclopedia of Genes and Genomes (KEGG) pathway enrichment analysis, which showed that YTHDF1-targeted transcripts were enriched for pathways associated with phagosomes and lysosomes (Fig. 3d). Limiting lysosomal proteolysis in DCs can enhance cross-presentation by minimizing destruction of internalized antigens[26,27]. We noticed that translation of a group of transcripts that encode lysosomal cathepsins, which are responsible for antigen degradation in DC lysosomes[26,27], was repressed in *Ythdf1*$^{-/-}$ DCs compared with wild-type DCs (Fig. 3e). By contrast, the translational efficacy of co-stimulatory or inhibitory molecules (signal 2) and cytokines (signal 3) was not substantially altered in YTHDF1-deficient FLT3L-DCs (Extended Data Fig. 6e). In line with the observation in FLT3L-DCs, loss of *Ythdf1* resulted in decreased translational efficiency of cathepsins in granulocyte–macrophage colony-stimulating factor (GM-CSF)-induced bone marrow DCs (GMDCs; Extended Data Fig. 7a–f). Consistently, we found that multiple cathepsin transcripts are bound by YTHDF1, and *Ythdf1* knockout resulted in significant decreases in the translation of these genes in both GMDCs and FLT3L-DCs (Extended Data Fig. 7g). These data suggest that lysosomal cathepsins are the main targets controlled by YTHDF1, and that they subsequently affect the cross-priming capacity of DCs.

Consistent with the reduced translational efficiency of m^{6}A-marked transcripts in *Ythdf1*$^{-/-}$ cDCs based on ribosome profiling, we also observed downregulation of cathepsins in *Ythdf1*$^{-/-}$ cDCs compared to wild-type cDCs in vivo (Fig. 4a) and in vitro (Extended Data Fig. 8a), although the decay of their transcripts was less affected by YTHDF1 depletion (Extended Data Fig. 8b). We reasoned that the reduced cathepsin levels could delay the degradation of the ingested neoantigens and facilitate sustained antigen release in endosomes or lysosomes, thereby contributing to the improved antigen presentation in *Ythdf1*$^{-/-}$ DCs. To test this hypothesis, we co-cultured GMDCs from wild-type and *Ythdf1*$^{-/-}$ mice with B16-OVA cells overnight and assessed purified DCs for intact residual OVA. We observed more residual intact OVA in *Ythdf1*$^{-/-}$ GMDCs than in *Ythdf1*$^{+/+}$ GMDCs (Extended Data Fig. 8c). We subsequently investigated whether the reduced translation efficiency of YTHDF1-target cathepsins affects cross-presentation in *Ythdf1*$^{-/-}$ DCs. Inhibition of cathepsins using the broad-spectrum

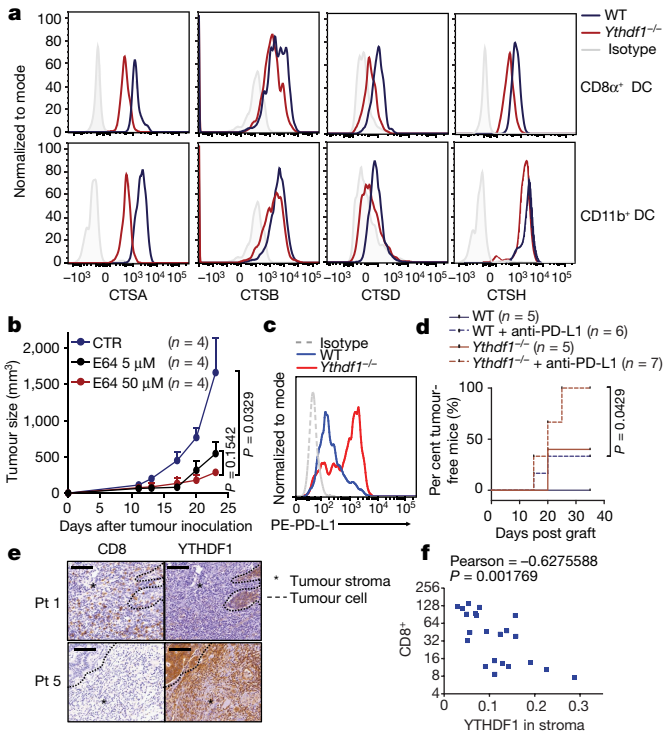

Fig. 4 | YTHDF1 promotes translation of proteases for excessive antigen degradation. a, Representative plots showing expression of cathepsins on splenic CD8α$^+$ and CD11b$^+$ cDCs from wild-type and *Ythdf1*$^{-/-}$ mice. **b**, Wild-type mice were injected subcutaneously with 10^6 B16-OVA cells. After 11 days, tumour-bearing mice were injected with DMSO as vehicle control (CTR) or E64 intratumorally (5 μM or 50 μM). Tumour growth was monitored over time. **c**, Wild-type and *Ythdf1*$^{-/-}$ mice were injected subcutaneously with 10^6 B16-zsGreen-OT1 tumour cells. PD-L1 expression on zsGreen$^+$ tumour cells is shown. **d**, Wild-type or *Ythdf1*$^{-/-}$ mice ($n = 5$ per group) were injected subcutaneously with 10^6 B16-OVA cells. Anti-PD-L1 antibody (200 μg) was administered on days 8 and 15. The percentage of mice with tumour regression was monitored over time and is shown as per cent tumour-free mice. **e**, Tissue sections from patients with colon cancer immunohistochemically stained for CD8 and YTHDF1. Dashed line shows edge of tumour. Asterisk marks stroma. Representative YTHDF1-low (Pt 1) and YTHDF1-high (Pt 5) specimens are shown. Scale bars, 100 μm. **f**, Correlations between the mean intensity of YTHDF1 in stroma area and the counts of CD8$^+$ cells are shown ($n = 22$ patients). Data are representative of two independent experiments with similar results (**a**, **c**); one of three representative images per tumour was shown (**e**). *n*, number of mice. Mean ± s.e.m., two-sided unpaired Student's *t*-test (**b**, **f**) or two-sided log-rank (Mantel–Cox) test (**d**).

cysteine protease inhibitor E64 or more selective inhibitors (CA-074 for cathepsin B and cathepsin L inhibitor III) notably enhanced the efficiency of cross-priming in wild-type DCs (Extended Data Fig. 8d–f). Moreover, the in vivo antitumour response was markedly improved by cathepsin blockade in wild-type mice (Fig. 4b, Extended Data Fig. 8g), suggesting that cathepsins are critical factors for determining the antitumour response in this model. Collectively, these data show that loss of YTHDF1 in DCs attenuates antigen degradation by restricting the expression of lysosomal proteases, leading to improved cross-presentation and better cross-priming of CD8$^+$ T cells.

Finally, we investigated whether loss of YTHDF1 with increased neoantigen-specific CD8$^+$ T cells could enhance the antitumour response to immune checkpoint blockade, which targets the T cell inhibitor receptor PD1. As *Ythdf1*$^{-/-}$ mice showed a marked increase in IFNγ in CD8$^+$ T cells, and IFNγ signalling upregulates the expression of PD-L1[28], the ligand for PD1, we evaluated the level of PD-L1. PD-L1 expression was increased in tumour cells from *Ythdf1*$^{-/-}$ tumour-bearing mice compared with wild-type mice (Fig. 4c), whereas neutralizing IFNγ diminished the expression of PD-L1 (Extended Data Fig. 9). We then tested whether PD-L1 blockade could potentiate the antitumour response in *Ythdf1*$^{-/-}$ mice. We treated wild-type and *Ythdf1*$^{-/-}$ tumour-bearing mice with an anti-PD-L1 antibody (clone 10F.9G2). Although tumour regression occurred in 40% of untreated *Ythdf1*$^{-/-}$ mice and anti-PD-L1-treated wild-type mice, 100% of anti-PD-L1-treated *Ythdf1*$^{-/-}$ mice showed complete tumour regression (Fig. 4d). These data suggest that combining a checkpoint blockade with YTHDF1 depletion could be a potential new therapeutic strategy to improve outcomes in patients with low response to checkpoint blockade.

In line with the observations in mouse models, we found that patients with colon cancer who had low expression of YTHDF1 in the tumour stroma tended to have a higher number of CD8$^+$ cells in tumour biopsies than patients with high expression of YTHDF1, who lacked CD8$^+$ cell infiltrates (Fig. 4e, f), further supporting the notion that the reduced YTHDF1 expression may correlate with the T cell inflamed tumour microenvironment.

Tumours can evade immune recognition despite expressing neoantigens. Our current results reveal that the m^{6}A-marked mRNAs that encode lysosomal proteases are recognized by YTHDF1 in DCs. Binding of YTHDF1 promotes translation of lysosomal proteases, suppressing the cross-presentation of engulfed tumour neoantigens, which represents a previously unrecognized (to our knowledge) mechanism of immune evasion. Our data do not exclude potential contributions from other targets of YTHDF1; further investigation of complex regulatory pathways mediated by the m^{6}A axis is necessary to expand our understanding and uncover additional features of antitumour immunity. Finally, this work suggests that YTHDF1 could be a therapeutic target for immunotherapy in combination with emerging checkpoint inhibitors or DC vaccines.

Online content

Any methods, additional references, Nature Research reporting summaries, source data, statements of data availability and associated accession codes are available at https://doi.org/10.1038/s41586-019-0916-x.

Received: 14 November 2017; Accepted: 10 January 2019;
Published online: 06 February 2019

1. Schumacher, T. N. & Schreiber, R. D. Neoantigens in cancer immunotherapy. *Science* **348**, 69–74 (2015).
2. Ott, P. A. et al. An immunogenic personal neoantigen vaccine for patients with melanoma. *Nature* **547**, 217–221 (2017).
3. Yarchoan, M., Johnson, B. A. III, Lutz, E. R., Laheru, D. A. & Jaffee, E. M. Targeting neoantigens to augment antitumour immunity. *Nat. Rev. Cancer* **17**, 209–222 (2017).
4. Sahin, U. et al. Personalized RNA mutanome vaccines mobilize poly-specific therapeutic immunity against cancer. *Nature* **547**, 222–226 (2017).
5. Wang, X. et al. *N*^{6}-methyladenosine modulates messenger RNA translation efficiency. *Cell* **161**, 1388–1399 (2015).
6. Desrosiers, R., Friderici, K. & Rottman, F. Identification of methylated nucleosides in messenger RNA from Novikoff hepatoma cells. *Proc. Natl Acad. Sci. USA* **71**, 3971–3975 (1974).
7. Dominissini, D. et al. Topology of the human and mouse m^{6}A RNA methylomes revealed by m^{6}A-seq. *Nature* **485**, 201–206 (2012).
8. Jia, G. et al. *N*^{6}-methyladenosine in nuclear RNA is a major substrate of the obesity-associated FTO. *Nat. Chem. Biol.* **7**, 885–887 (2011).
9. Meyer, K. D. et al. Comprehensive analysis of mRNA methylation reveals enrichment in 3′ UTRs and near stop codons. *Cell* **149**, 1635–1646 (2012).
10. Wang, X. et al. *N*^{6}-methyladenosine-dependent regulation of messenger RNA stability. *Nature* **505**, 117–120 (2014).
11. Barbieri, I. et al. Promoter-bound METTL3 maintains myeloid leukaemia by m^{6}A-dependent translation control. *Nature* **552**, 126–131 (2017).
12. Li, Z. et al. FTO plays an oncogenic role in acute myeloid leukemia as a *N*^{6}-Methyladenosine RNA demethylase. *Cancer Cell* **31**, 127–141 (2017).
13. Vu, L. P. et al. The *N*^{6}-methyladenosine (m^{6}A)-forming enzyme METTL3 controls myeloid differentiation of normal hematopoietic and leukemia cells. *Nat. Med.* **23**, 1369–1376 (2017).
14. Liu, J. et al. m^{6}A mRNA methylation regulates AKT activity to promote the proliferation and tumorigenicity of endometrial cancer. *Nat. Cell Biol.* **20**, 1074–1083 (2018).
15. Shi, H. et al. m^{6}A facilitates hippocampus-dependent learning and memory through YTHDF1. *Nature* **563**, 249–253 (2018).
16. Yadav, M. et al. Predicting immunogenic tumour mutations by combining mass spectrometry and exome sequencing. *Nature* **515**, 572–576 (2014).
17. Mellman, I., Coukos, G. & Dranoff, G. Cancer immunotherapy comes of age. *Nature* **480**, 480–489 (2011).

18. Jongbloed, S. L. et al. Human CD141$^+$ (BDCA-3)$^+$ dendritic cells (DCs) represent a unique myeloid DC subset that cross-presents necrotic cell antigens. *J. Exp. Med.* **207**, 1247–1260 (2010).
19. Spranger, S., Bao, R. & Gajewski, T. F. Melanoma-intrinsic β-catenin signalling prevents anti-tumour immunity. *Nature* **523**, 231–235 (2015).
20. Naik, S. H. et al. Cutting edge: generation of splenic CD8$^+$ and CD8$^-$ dendritic cell equivalents in Fms-like tyrosine kinase 3 ligand bone marrow cultures. *J. Immunol.* **174**, 6592–6597 (2005).
21. Mayer, C. T. et al. Selective and efficient generation of functional Batf3-dependent CD103$^+$ dendritic cells from mouse bone marrow. *Blood* **124**, 3081–3091 (2014).
22. Kretzer, N. M. et al. RAB43 facilitates cross-presentation of cell-associated antigens by CD8α$^+$ dendritic cells. *J. Exp. Med.* **213**, 2871–2883 (2016).
23. Driessens, G., Kline, J. & Gajewski, T. F. Costimulatory and coinhibitory receptors in anti-tumor immunity. *Immunol. Rev.* **229**, 126–144 (2009).
24. Fuertes, M. B. et al. Host type I IFN signals are required for antitumor CD8$^+$ T cell responses through CD8α$^+$ dendritic cells. *J. Exp. Med.* **208**, 2005–2016 (2011).
25. Woo, S. R. et al. STING-dependent cytosolic DNA sensing mediates innate immune recognition of immunogenic tumors. *Immunity* **41**, 830–842 (2014).
26. Cebrian, I. et al. Sec22b regulates phagosomal maturation and antigen crosspresentation by dendritic cells. *Cell* **147**, 1355–1368 (2011).
27. Samie, M. & Cresswell, P. The transcription factor TFEB acts as a molecular switch that regulates exogenous antigen-presentation pathways. *Nat. Immunol.* **16**, 729–736 (2015).
28. Benci, J.L. et al. Tumor interferon signaling regulates a multigenic resistance program to immune checkpoint blockade. *Cell* **167**, 1540–1554 (2016).
29. Tripathi, S. et al. Meta- and orthogonal integration of influenza "OMICs" data defines a role for UBR4 in virus budding. *Cell Host Microbe* **18**, 723–735 (2015).

Acknowledgements This study was supported by the National Key Research and Development Program of China, Stem Cell and Translational Research (2018YFA0109700 to D.H.), Strategic Priority Research Program of the Chinese Academy of Science (XDA16010404 to D.H.), National Institute of Health (HG008935 and GM113194 to C.H.), Ludwig Center at the University of Chicago (to C.H. and R.R.W.), CAS Hundred Talent Program (to D.H.), National Natural Science Foundation of China (31870890 to M.M.X., 31741074 to D.H.), National Science Fund for Excellent Young Scholars (31622039 to B.S.), Science Foundation for Distinguished Young Scholars of Jiangsu Province (BK20160045 to B.S.) and Open Project of Key Laboratory of Genomic and Precision Medicine of the CAS. The Mass Spectrometry Facility of the University of Chicago is funded by National Science Foundation (CHE-1048528). C.H. is an investigator of the Howard Hughes Medical Institute. We thank J. Tauler for editing.

Reviewer information *Nature* thanks J. Hanna, J. Neefjes and the other anonymous reviewer(s) for their contribution to the peer review of this work.

Author contributions D.H. and M.M.X. conceived the project. D.H., M.M.X., J.L., L.D., X.H., Y.L. and R.C. performed experimental work. D.H. and C.C. performed bioinformatics analysis. Y.L., J.W. and B.S. generated *Ythdf1* knockout mice. M.B.B. and U.D. provided human colon biopsy samples. D.H., M.M.X. and C.H. designed the study. D.H., M.M.X., C.H. and R.R.W. wrote the manuscript with input from all authors.

Competing interests C.H. is a scientific founder and a member of the scientific advisory board of Accent Therapeutics, Inc. A patent application on YTHDF1 has been filed by the University of Chicago.

Additional information
Extended data is available for this paper at https://doi.org/10.1038/s41586-019-0916-x.
Supplementary information is available for this paper at https://doi.org/10.1038/s41586-019-0916-x.
Reprints and permissions information is available at http://www.nature.com/reprints.
Correspondence and requests for materials should be addressed to D.H. or M.M.X. or C.H.
Publisher's note: Springer Nature remains neutral with regard to jurisdictional claims in published maps and institutional affiliations.

METHODS

Mice. *Ythdf1*$^{-/-}$ mice were generated as previously described[15]. Founder mice with mutant alleles were backcrossed to C57BL/6J mice for two generations. Mice used for experiments were further backcrossed to C57BL/6J mice for seven generations (total nine generations). To ensure comparability in genetic background, mice were maintained by crossing heterozygous and heterozygous mice. *Ythdf1*$^{-/-}$ mice or their littermate control wild-type mice were used in all experiments. Littermates were co-housed during experiments to reduce variation in microbiome and environment. Primers used for genotyping of *Ythdf1*$^{-/-}$ mice: CACCTGAGTTCAGATCATTAC and GCTCCAGACTGTTCATCC. Female *Rag2*$^{-/-}$ mice and 2C CD8^{+} TCR transgenic, Cd11c-Cre and *Zbtb46*-DTR mice were purchased from Jackson laboratory. Female CD11c-*CreMettl14*$^{f/f}$ conditional knockout mice were generated in-house. All mice were used at 6–12 weeks of age. All mice were maintained under specific pathogen-free conditions and used in accordance with the animal experimental guidelines set by the Institute of Animal Care and Use Committee. This study has been approved by the Institutional Animal Care and Use Committee of The University of Chicago.

Cell lines. MC38 is a mouse colon adenocarcinoma cell line that was provided by D. Bartlett (University of Pittsburgh, Pittsburgh). B16-OVA, an OVA-transfected clone derived from the mouse melanoma cell line B16, was provided by Y.-X. Fu (UT Southwestern). The B16F10 cell line was purchased from ATCC. MC38-zsGreen-OTIp (MC38-OZ) and B16F10-zsGreen-OTIp (B16-OZ) were selected for a single clone after being transduced by lentivirus expressing zsGreen-OTIp (SIINFEKEL). MC38-SIY is an EGFR-SIY-transfected clone derived from the mouse colon cell line MC38. Cells were maintained in Dulbecco's modified Eagle's medium (DMEM; Invitrogen) supplemented with 10% FBS, 1% penicillin-streptomycin, 2 mM L-glutamine, 1 mM sodium pyruvate and 0.1 mM non-essential amino acids at 37 °C in 5% CO_2.

Primary cell cultures. Single-cell suspensions of BMCs were cultured in RPMI-1640 medium containing 10% fetal bovine serum, supplemented with 20 ng/ml GM-CSF (Biolegend). Fresh medium with GM-CSF was added into culture on days 3 and 5. On day 6, CD11c^{+} DCs were purified using the EasySep Mouse CD11c Positive Selection Kit II (STEMCELL Technologies). To culture FLT3L-DCs, single-cell suspensions of BMCs were cultured in Iscove's modified Dulbecco's medium (IMDM) containing 10% fetal bovine serum at a concentration of 1×10^6 per ml. Cells were supplemented with 100 ng/ml FLT3L (PEPROTECH) for 9–10 days to obtain FLT3L-DCs.

Tumour growth and treatments. B16-OVA or MC38 tumour cells (1×10^6) were injected subcutaneously (s.c.) into the flank of mice. Tumour volumes were measured by length (a) and width (b) and calculated as tumour volume $= ab^2/2$. Mice with tumour volumes less than 200 mm^3 are considered to be surviving. For the in vivo depletion study, 200 μg of anti-CD8 antibody (clone YTS169.4) or anti-NK1.1 (clone PK136) was injected intraperitoneally (i.p.) three days after tumour inoculation. To block cathepsins in vivo, mice were inoculated with 1×10^6 B16-OVA cells. On day 11, mice with established tumours were treated with E64 intratumorally. For anti-PD-L1 treatment, 1×10^6 B16-OVA tumour cells were s.c. injected into the flank of mice. Tumours were allowed to grow for seven days and treated i.p. with anti-PD-L1 (clone10F.9G2) or rat immunoglobulin. Tumour-free mice after treatment were monitored over time and the percentage of tumour regression was calculated. To block IFNγ, tumour-bearing mice were treated with 50 μg anti-IFNγ monoclonal antibody (clone XMG1.2) intratumorally and PD-L1 expression on tumour cells was evaluated by flow cytometry. All antibodies were InVivoMAb from BioXCell. For adoptive transfer of T cells, Rag mice were inoculated with 5×10^5 B16-OVA on day 0. On the same day, T cells were purified from wild-type or *Ythdf1*$^{-/-}$ mice using a T cell negative isolation kit (STEMCELL Technologies). T cells (5×10^6) were injected intravenously (i.v.) into *Rag2*$^{-/-}$ mice. Tumour-bearing mice were killed before the tumour diameter reached 2 cm; this tumour size limit was approved by the Institutional Animal Care and Use Committee of The University of Chicago.

Generation of bone marrow chimaera. To generate bone marrow chimeric mice, C57BL/6 mice were exposed to 8 Gy of X-ray radiation. After 24 h, 5×10^6 BMCs, consisting of 2.5×10^6 wild-type or *Ythdf1*$^{-/-}$ BMCs and 2.5×10^6 *Zbtb46*-DTR BMCs, were injected i.v. into irradiated mice. Six weeks after reconstitution, *Zbtb46*-DTR:*Ythdf1*$^{+/+}$ and *Zbtb46*-DTR:*Ythdf1*$^{-/-}$ mixed bone marrow chimaera mice were inoculated with 10^6 B16-OVA cells and treated with 400 ng diphtheria toxin (Sigma) or PBS every other day for 16 days.

Flow cytometry and cell sorting. For flow cytometric analysis and cell sorting, tumours, lymph nodes and spleens were collected from mice and digested with 0.26 U/ml Liberase TM and 0.25 mg/ml DNase I at 37 °C for 30 min. Samples were then filtered through a 70-μm cell strainer and washed twice with staining buffer. Cells were re-suspended in staining buffer (PBS with 2% FCS and 1 mM EDTA). Cells were incubated with Fc Block (clone 2.4G2; BioX Cell) for 10 min. Subsequently, specific antibodies were added and staining was continued for 30 min on ice. Information about all the antibodies used is provided in Supplementary Table 1. OT-I-specific T cells were stained using iTAg Tetramer/H-2K^{b}OVA (SIINFEKEL) (MBL). After a washing step, cells were either analysed on a BD Fortessa (BD) or sorted by AriaIIIu (BD). For the staining of cathepsins, splenocytes were stained with CD11c, B220, MHCII, CD8 and CD11b and then fixed with 4% PFA (Biolegend) for 30 min. Fixed cells were then washed twice with the 1× intracellular staining perm and wash buffer (Biolegend). Antibodies against CTSA, CTSB, CTSD or CTSH were added and incubated overnight. Alexa Fluor 568 goat anti-rabbit IgG was added as the secondary antibody. CD11c^{+} MHCII^{+}B220^{-} was gated and the expression of cathepsins was evaluated by fluorescence intensity. Analysis of flow cytometry data was performed using Flowjo (Treestar).

Measurement of IFNγ-secreting CD8^{+} T cells by ELISPOT assay. For antigen-specific CD8^{+} T cell functional assay in the B16-OVA model, 12 days after tumour inoculation, 3×10^5 lymphocytes were re-stimulated with 1 μg/ml SIINFEKEL or MC38 tumour cells (lymphocyte:MC38 = 50:1) for 48 h. A 96-well HTS-IP plate (Millipore) was pre-coated with anti-IFNγ antibody (BD Bioscience) with a 1:250 dilution overnight at 4 °C. After co-culture, cells were removed. Biotinylated anti-IFNγ antibody (2 mg/ml; BD Bioscience) with a 1:250 dilution was added and incubated for 2 h at room temperature or overnight at 4 °C. Avidin-horseradish peroxidase (BD Bioscience) with a 1:1,000 dilution was then added and the plate was incubated for 1 h at room temperature. IFNγ spots were developed according to the manufacturer's instructions (BD Bioscience).

Antigen-presentation assay. For cross-presentation of tumour neoantigens, CD11b^{+} or CD8^{+} DCs were purified from DLNs of wild-type or *Ythdf1*$^{-/-}$ mice 6 days after inoculation with B16-OVA, MC38-OTIp or MC38-EGFR-SIY. OT-I or 2C naive CD8^{+} T cells were isolated from lymph nodes and spleen of 6- to 12-week-old mice. Negative selection was carried out with a negative CD8 isolation kit (STEMCELL Technologies) following the manufacturer's instructions. DCs were co-cultured with OT-I naive CD8 T cells at a ratio of 1:10 for three days with or without 1 μg/ml SIINFEKEL peptide. For cross-presentation of soluble OVA, splenic DCs were sorted and stimulated with 100 ng/ml LPS overnight. DCs were then pulsed with different concentrations of OVA (endotoxin free, Sigma) for 5 h. Cells were washed and co-cultured with OT-I naive CD8^{+} T cells for three days. For in vitro cross-presentation of tumour neoantigen, FLT3L-DCs were collected on days 9–10 and co-cultured with necrotic B16-OVA tumour cells overnight. B220^{-}CD11c^{+} cells were subsequently purified. GMDCs from *Mettl14*$^{f/f}$ or CD11c-Cre*Mettl14*$^{f/f}$ mice were collected on day 6 and co-cultured with necrotic B16-OVA tumour cells for 16 h. To inhibit cathepsins, GMDCs were pre-treated with E64 (sigma) for 2 h followed by co-culturing with tumour cells. CD11c^{+} cells were then purified and incubated with naive CD8^{+} T cells from OT-I mice for three days. IFNγ production was detected using an IFNγ Flex Set CBA assay (BD Bioscience). To inhibit cathepsins in ex vivo cDCs, wild-type or *Ythdf1*$^{-/-}$ mice were inoculated with 5×10^5 MC38 cells. Thirty-six hours after tumour inoculation, spleens were removed and digested, and CD11c^{+} DCs were purified using the EasySep Mouse CD11c Positive Selection Kit II (STEMCELL Technologies). CD11c^{+} DCs were then treated with 0.04 μM E64 (Sigma) overnight followed by co-culturing with OVA protein for 4 h. Any free OVA protein was then removed from the culture medium, and CD11c^{+} cells were incubated with cell-trace violet (CTV)-labelled OT-I cells for three days. The cross-priming capacity of DCs was analysed by the dilution of CTV in CD8^{+} T cells. For the in vitro cathepsin inhibition assay, FLT3L-DCs were treated with 5 μg/ml CA-074 methyl ester (Selleck), 5 μg/ml cathepsin L inhibitor III (Sigma) or a combination (5 μg/ml CA-074 methyl ester and 5 μg/ml cathepsin L inhibitor III) for 2 h followed by co-culturing with necrotic B16-OVA cells for 16 h, and then FLT3L-DCs were purified using an EasySep Mouse CD11c Positive Selection Kit II (STEMCELL Technologies). The purified cells were incubated with OT-I cells at a ratio of 1:20 for three days. The cross-priming capacity of DCs was then measured by IFNγ production. To detect MHC-H2K^{b}-SIINFEKEL, mice were inoculated with B16-OVA. After 12 days, tumours were removed and tumour-infiltrating DCs (CD45^{+}CD11b^{+}Ly6C^{-}MHCII^{+}CD24^{+}CD11c^{+}) were stained with monoclonal antibody 25.D1.

Cell trace violet labelling. Ten million splenocytes from naive OT-I mice were re-suspended in 1 ml PBS followed by incubating with 5 μM CTV (ThermoFisher) at 37 °C for 20 min. RPMI-1640 medium (5 ml) was added to the cells and incubated for 5 min to remove the free dye in the solution. These cells were then centrifuged and incubated with pre-warmed RPMI-1640 for at least 10 min at room temperature for subsequent analysis.

RIP– seq. Twenty million GMDCs were harvested and co-cultured with or without necrotic B16-OVA overnight. The procedure was adapted from a previous report[10]. Five million FLT3L-DCs were harvested. DCs were then purified and pelleted by centrifuge for 5 min. Cells were washed twice with cold PBS and the cell pellet was re-suspended with two volumes of lysis buffer (150 mM KCl, 10 mM HEPES pH 7.6, 2 mM EDTA, 0.5% NP-40, 0.5 mM dithiothreitol (DTT), 1:100 protease inhibitor cocktail, 400 U/ml RNase inhibitor). The lysate was incubated on ice for 5 min and centrifuged for 15 min to clear the lysate. One-tenth volume of cell lysate was saved as input and total RNA was extracted using Trizol. The rest of the

cell lysate was incubated with 5 μg anti-YTHDF1 (Proteintech) at 4 °C overnight with gentle rotation followed by incubation with 40 μl protein G beads for 1 h at 4 °C. The beads were then washed five times with 1 ml ice-cold washing buffer (200 mM NaCl, 50 mM HEPES pH 7.6, 2 mM EDTA, 0.05% NP-40, 0.5 mM DTT, 200 U/ml RNase inhibitor). The immunoprecipitation complex was resuspended in 400 μl 1 × Proteinase K and digested with 2 mg Proteinase K at 55 °C for 1 h. RNA was then extracted using an RNA isolation kit (Zymo). Input and immunoprecipitated RNA of each sample were used to generate the library using a TruSeq stranded mRNA sample preparation kit (Illumina).

m^{6}A-seq. Total RNA was isolated from DCs. Polyadenylated RNA was further enriched from total RNA using the Dynabeads mRNA Purification Kit (Invitrogen). RNA samples were fragmented into ~100-nucleotide-long fragments by sonication. Fragmented RNA (100 ng mRNA or 5 μg total RNA) was used for m^{6}A immunoprecipitation (m^{6}A-IP) with the EpiMark N^6-methyladenosine enrichment kit (NEB E1610S) according to the manufacturer's protocol. RNA was enriched through RNA Clean & Concentration-5 (Zymo Research) and used for library generation with SMARTer Stranded Total RNA-Seq Kit (Takara). Sequencing was performed at the University of Chicago Genomics Facility on an Illumina HiSeq4000 machine in single-read mode with 50 bp per read. Sequencing reads were aligned to the mouse genome mm9 by STAR (version 2.6.0c)[30]. The m^{6}A-enriched regions (peaks) in each m^{6}A-IP sample were detected by MACS2 (version 2.1.1.20160309)[31] with $q < 0.01$ and the corresponding m^{6}A-input sample was used as the control. Peaks that were detected by both replicates were considered as high-confidence peaks. The peak annotation and binding motif were analysed by HOMER (version 4.9)[29].

Ribosome profiling. DCs (5×10^6) were treated with 100 μg/ml cycloheximide (CHX) for 7 min. The cells were then harvested using a cell lifter. The cell suspension was spun at 400*g* for 5 min and the cell pellet was washed twice with 5 ml cold PBS with CHX (100 μg/ml). Lysis buffer (200 μl; 10 mM Tris, pH 7.4, 150 mM KCl, 5 mM $MgCl_2$, 100 μg/ml CHX, 0.5% Triton-X-100, freshly added 1:100 protease inhibitor, 40 U/ml SUPERasin) was added to the cell pellet and the pellet was lysed on ice for 15 min with rotation. Ten per cent of the clarified lysate was saved as input and the rest of the lysate was separated through a 5 ml 10–50% sucrose gradient and centrifuged at 4 °C for 2 h at 28,000 r.p.m. Fractions were collected separately and analysed using a Qubit RNA HS Assay Kit (Invitrogen). The fractions corresponding to monosome or polysome, respectively, were combined and concentrated on Amicon-Ultra 100K columns (Millipore). Two A260 units of ribosome fractions were digested with 60 U RNase I (Ambion) at room temperature for 30 min. RNA was extracted using RNA Clean & Concentrate (Zymo) and ribosomal RNA was deleted before size selection. RNA fragments (26–32 nt) were isolated using 15% denaturing Urea-PAGE gel. RNA was eluted from gel in elution buffer (300 mM sodium acetate pH 5.2, 1 mM EDTA) followed by phenol-chloroform extraction and ethanol precipitation. RNA fragments were dephosphorylated and prepared into libraries using a SMARTer smRNA-Seq Kit (Clontech). The first three bases of sequencing reads were removed using fastx_trimmer (version 0.0.14). The adaptor sequences and polyA tails were first trimmed from sequencing reads by using cutadapt (version 1.15) with parameters –minimum-length 18 -n 3 -a "AAAAAAAAAAAAAA" -a "AGATCGGAAGAGCACACGTCTGAACTCCAGTCAC"[32]. Trimmed reads were filtered for mitochondrial DNA and ribosomal RNA using Bowtie2 (version 2.3.4)[33]. All remaining reads were mapped to the mouse genome mm9 using STAR (version 2.6.0c)[30]. Uniquely mapped reads were selected using SAMtools (version 1.7)[34] with mapping quality ≥ 20, and then removing duplication. The raw counts of coding regions were calculated using HOMER (version 4.9)[29]. Genes with differential translational efficiency[35] (TE) as defined in equation (1) were detected using Bioconductor DESeq2 package (version 1.18.1)[36] with adjusted $P \leq 0.1$ and fold change ≥ 0.5.

$$\mathrm{TE} = \frac{\frac{\textit{Ythdf1}^{-/-}\ \text{(ribosome)}}{\textit{Ythdf1}^{-/-}\ \text{(RNA-seq)}}}{\frac{\text{Wild-type (ribosome)}}{\text{Wild-type (RNA-seq)}}} \quad (1)$$

Measurement of RNA lifetime. DCs were seeded in 24-well plates at 50% confluency. After 2 h, actinomycin D was added to 5 mg/ml at 3 h, 2 h, 1 h and 0 h before collection. The total RNA was purified by RNeasy kit with an additional DNase-I digestion step on the column. RNA quantities were determined using quantitative PCR with reverse transcription (RT–qPCR). The specific primers used are as follows: *Ctsb*_Forward: CTGCTTACCATACACCAT, *Ctsb*_Reverse: TCCTTCACACTGTTAGAC; *Ctsd*_Forward: GGCAAGAGGTATCAAGGT, *Ctsd*_Reverse: CAGGTAGAAGGAGAAGATGT; *Ctsl*_Forward: GAGTTCGCTGTGGCTAAT, *Ctsl*_Reverse: GAGGTTCTTGCTGCTACA; *Gapdh*_Forward: ACCTGCCAAGTATGATGA, *Gapdh*_Reverse: GGAGTTGCTGTTGAAGTC.

Immunohistochemistry of human biopsies. All samples of tumour biopsies from 22 colorectal cancer patients were obtained with informed consent under a protocol approved by the University of Chicago Institutional Review Board. We complied with all relevant ethical regulations. Information about the sex, age, and tumour characteristics of patients are given in Supplementary Table 2. To stain for YTHDF1 and CD8, antigen retrieval was performed with 10 mM Tris base, 1 mM EDTA, 0.05% Tween 20, pH 9. Slides were processed with the VECTASTAIN Elite ABC HRP Kit and DAB Substrate Kit (Vector Laboratories). Slides were counterstained with haematoxylin and dehydrated through graded alcohols and xylene. A total of 22 tumour samples had sufficient tissue for unambiguous analyses; for immunohistochemical (IHC) quantification, DAB stains of IHC images were separated using colour deconvolution algorithms[47] in Fiji, a derivative of ImageJ. The mean DAB intensity of three random images at 795 × 650 pixels was calculated and converted into optical density (OD). CD8-positive cells were analysed using Image J cell counter. The average infiltration of CD8$^+$ cells and average expression of YTHDF1 in the surrounding stroma tissue were assessed.

Western blot analysis. To detect the expression of cathepins, GMDCs were harvested on day 6 and co-cultured with necrotic B16-OVA cells at a ratio of 1:1 for 16 h. CD11c$^+$ DCs were then purified. Equal numbers of cells were lysed on ice for 15 min using 1 × lysis buffer (CST) supplemented with a protease inhibitor cocktail (Calbiochem). The cell lysis solution was centrifuged at 16,100*g* at 4 °C for 15 min. Clarified supernatant was loaded into 4–12% NuPAGE Bis-Tris gel and transferred to PVDF membranes (Life Technologies). Membranes were blocked for 1 h in 5% milk TBST and then incubated with primary antibodies in the blocking buffer overnight at 4 °C. After being washed five times, membranes were incubated with secondary antibodies for 1 h at room temperature. Information about all antibodies used is provided in Supplementary Table 1.

Degranulation of tumour infiltrating NK cells. Tumour-infiltrating leukocytes were resuspended at 5×10^5 per ml and stimulated with phorbol-12-myristate-13-acetate (PMA) (2.5 μg/ml) and ionomycin (0.5 μg/ml) in 96-well plates. CD107α-PE antibody and 1 × bredeldin A (Biolegend) were added directly to the wells and incubated for 4 h at 37 °C in 5% CO_2. Cells were stained for CD45 and NK1.1 (BD Biosciences) for 30 min. Samples were washed and then fixed in 1% paraformaldehyde.

Phagocytosis in vivo. B16F10 cells (5×10^5) expressing zsGreen-OTI were injected s.c. into wild-type and *Ythdf1*$^{-/-}$ mice. Tumour tissues were removed and digested.

Maturation of DCs. GMDCs were collected and co-cultured with 100 ng/ml LPS overnight. Cytokine production was measured using the Mouse Inflammation Kit (BD).

Identification of off-target site and T7EI assay. Two identified off-target loci for each sgRNA site with the highest scores were selectively amplified using the following primers: YTHDF1_For: TGACATTGGTGGCCATATCTGTC; YTHDF1_Rev: TGTCTGCCCATCAACAACTGTGC; Tex52_For: AGGATGAGAGG TGTTCAGCTAGAC; Tex52_Rev: TCTGTAGGCCCAGAGTCCTCAG; Nrp2_For: AGGGTAATACTACCACACATCAACCG; Nrp2_Rev: AGAGCTGGGGTCTAAT TGAATTTGGG; Eme1_For: TGCTGTCTCGCCTCGCAATAGC; Eme1_Rev: TGCGTACACTTAAGTCTGCCTGG; MED20_For: TCAAGGGCTTCTTCCA GAGTGCC; MED20_Rev: AGGCACCACACAAACCAGGCAAG. A HiPure Tissue DNA Mini Kit (Magen, D3121-03) was used to extract genomic DNA from the tails of wild-type and *Ythdf1*$^{-/-}$ mice. PCR reactions to amplify 350-bp fragments (for *Ythdf1*$^{-/-}$ mice) and 510-bp fragmentd (for wild-type mice) were carried out in 30-μl reactions, using 15 μl of 2 × EasyTaq PCR SuperMix (AS111 TransGen Biotech), 0.75 μM each of forward and reverse primers and 1 μl genomic DNA. The reaction products were subjected to 1.5% agarose gel electrophoresis. For the T7E1 cleavage assay, equal volumes of PCR products from *Ythdf1*$^{-/-}$ and wild-type mice were mixed and then denatured and annealed in NEBuffer 2 (NEB) using a thermal cycler. Hybridized PCR products were digested with T7 endonuclease I (NEB, M0302L) or ddH2O (as control) for 20 min at 37 °C and subjected to 1.5% agarose gel electrophoresis.

Statistical analysis and reproducibility. No statistical method was used to predetermine sample size. Mice were assigned at random to treatment groups for all mouse studies and, where possible, mixed among cages. No mice were excluded from experiments. Blinded staining and blinded analysis were performed for IHC experiments. Experiments were independently repeated two to three times. Data were analysed using Prism 5.0 software (GraphPad) and presented as mean values ± s.e.m. *P* values were calculated using one-sided or two-sided unpaired Student's *t*-tests. For survival curves, the log-rank (Mantel–Cox) test was used. For translational efficiency, *P* values were calculated using the likelihood ratio test and adjusted by the Benjamini–Hochberg method. For cumulative distribution, the two-sided Kolmogorov–Smirnov test was used to calculate *P* values.

Data processing and analysis. Illumina reads were post-processed and aligned to the mouse mm9 assembly using STAR[30] (version 2.6.0c) with default parameters. To visualize sequencing signals in the genome browser, we generated RIP-seq and m^{6}A-seq bigwig files with bamCoverage function from deepTools (version 3.0.1)[37] with '-bs = 1–normalizeUsing BPM'. For RIP-seq, Piranha software (version 1.2.1)[38]

was to detect the binding sites of YTHDF1 with '-b 100 -i 100'. Metagene plots were created using the Bioconductor GUITAR[39] package (version 1.16.0). Peaks that were detected by both replicates were considered as high-confidence peaks. GO term analyses were performed using metascape[40].

Reporting summary. Further information on research design is available in the Nature Research Reporting Summary linked to this article.

Data availability

The data that support the findings of this study are available from the corresponding author upon reasonable request. RIP–seq, Ribo-seq and m^{6}A-seq datasets have been deposited in the Gene Expression Omnibus (GEO) under the accession number GSE115106. A summary of sequencing experiments is provided in Supplementary Table 3. The differential translational efficiency results provided in Supplementary Table 4. Source Data for bar graphs and box-plots in the Figures and Extended Data Figures are provided in separate Excel files.

30. Dobin, A. et al. STAR: ultrafast universal RNA-seq aligner. *Bioinformatics* **29**, 15–21 (2013).
31. Zhang, Y. et al. Model-based analysis of ChIP-Seq (MACS). *Genome Biol.* **9**, R137 (2008).
32. Martin, M. Cutadapt removes adapter sequences from high-throughput sequencing reads. *Embnet J.* **17**, 10–12 (2011).
33. Langmead, B. & Salzberg, S. L. Fast gapped-read alignment with Bowtie 2. *Nat. Methods* **9**, 357–359 (2012).
34. Li, H. et al. The sequence alignment/map format and SAMtools. *Bioinformatics* **25**, 2078–2079 (2009).
35. Ingolia, N. T., Lareau, L. F. & Weissman, J. S. Ribosome profiling of mouse embryonic stem cells reveals the complexity and dynamics of mammalian proteomes. *Cell* **147**, 789–802 (2011).
36. Love, M. I., Huber, W. & Anders, S. Moderated estimation of fold change and dispersion for RNA-seq data with DESeq2. *Genome Biol.* **15**, 550 (2014).
37. Ramirez, F., Dundar, F., Diehl, S., Gruning, B. A. & Manke, T. deepTools: a flexible platform for exploring deep-sequencing data. *Nucleic Acids Res.* **42**, W187–W191 (2014).
38. Uren, P. J. et al. Site identification in high-throughput RNA-protein interaction data. *Bioinformatics* **28**, 3013–3020 (2012).
39. Cui, X. et al. Guitar: An R/Bioconductor package for gene annotation guided transcriptomic analysis of RNA-related genomic features. *BioMed Res. Int.* **2016**, 8367534 (2016).
40. Heinz, S. et al. Simple combinations of lineage-determining transcription factors prime *cis*-regulatory elements required for macrophage and B cell identities. *Mol. Cell* **38**, 576–589 (2010).

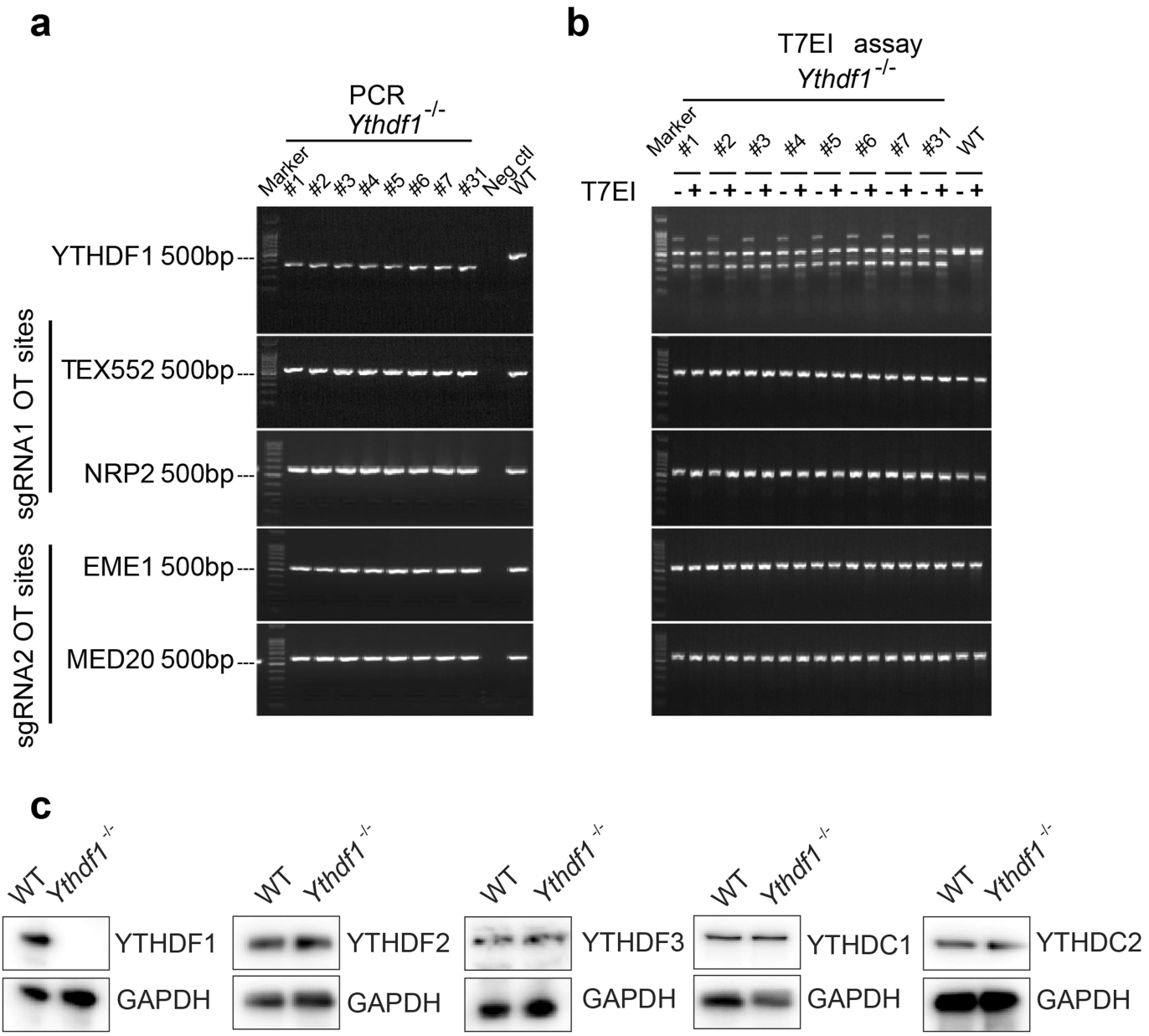

Extended Data Fig. 1 | Deletion efficacy of *Ythdf1*$^{-/-}$ mice. a, **b**, Off-target analysis of the CRISPR–Cas9 system in *Ythdf1*$^{-/-}$ mice. **a**, *Ythdf1* single guide RNA (sgRNA) targeting sites and four putative off-target sites were amplified. **b**, PCR products from *Ythdf1*$^{-/-}$ mice and wild-type mice were mixed and digested by T7EI. The PCR product from wild-type mice was used as negative control. **c**, Immunoblot assays are shown to validate changes in YTH protein expression in *Ythdf1*$^{-/-}$ DCs. Data are representative of one experiment (**a**, **b**) and two independent biological replications (**c**).

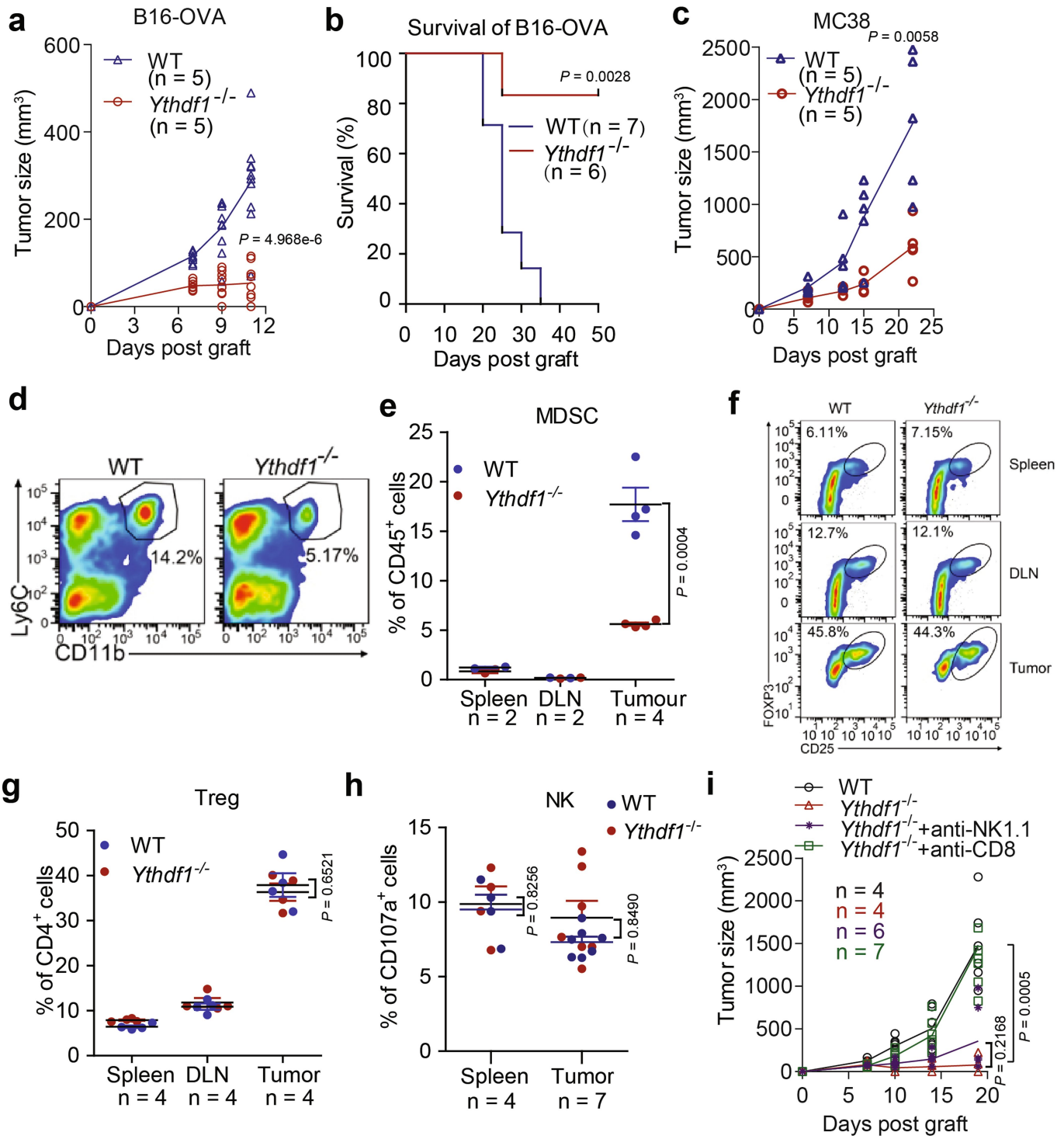

Extended Data Fig. 2 | Characterization of immune phenotypes of *Ythdf1*$^{-/-}$ mice. **a**, Data points for Fig. 1a. **b**, Wild-type or *Ythdf1*$^{-/-}$ mice were injected s.c. with 10^6 B16-OVA cells. Survival was monitored. Mice with tumour volumes less than 200 mm^3 are considered to be surviving. One of three representative experiments is shown. **c**, Data points for Fig. 1b. **d**–**h**, Wild-type or *Ythdf1*$^{-/-}$ mice were injected s.c. with 10^6 B16-OVA cells. **d**, **e**, Frequency of tumour infiltrating MDSCs (Ly6C$^+$CD11b$^+$) was assessed 12 days after tumour inoculation. **f**, **g**, The percentages of T_{reg} cells in spleen, DLN and tumour are shown. **h**, Degranulation of tumour NK cells in response to in vitro re-stimulation with PMA/ionomycin. **i**, Data points for Fig. 1d. Data are representative of two independent experiments (**a**, **c**). *n*, number of mice. Mean ± s.e.m., two-sided unpaired Student's *t*-test (**a**, **c**, **e**, **g**–**i**); two-sided log-rank (Mantel–Cox) test (**b**).

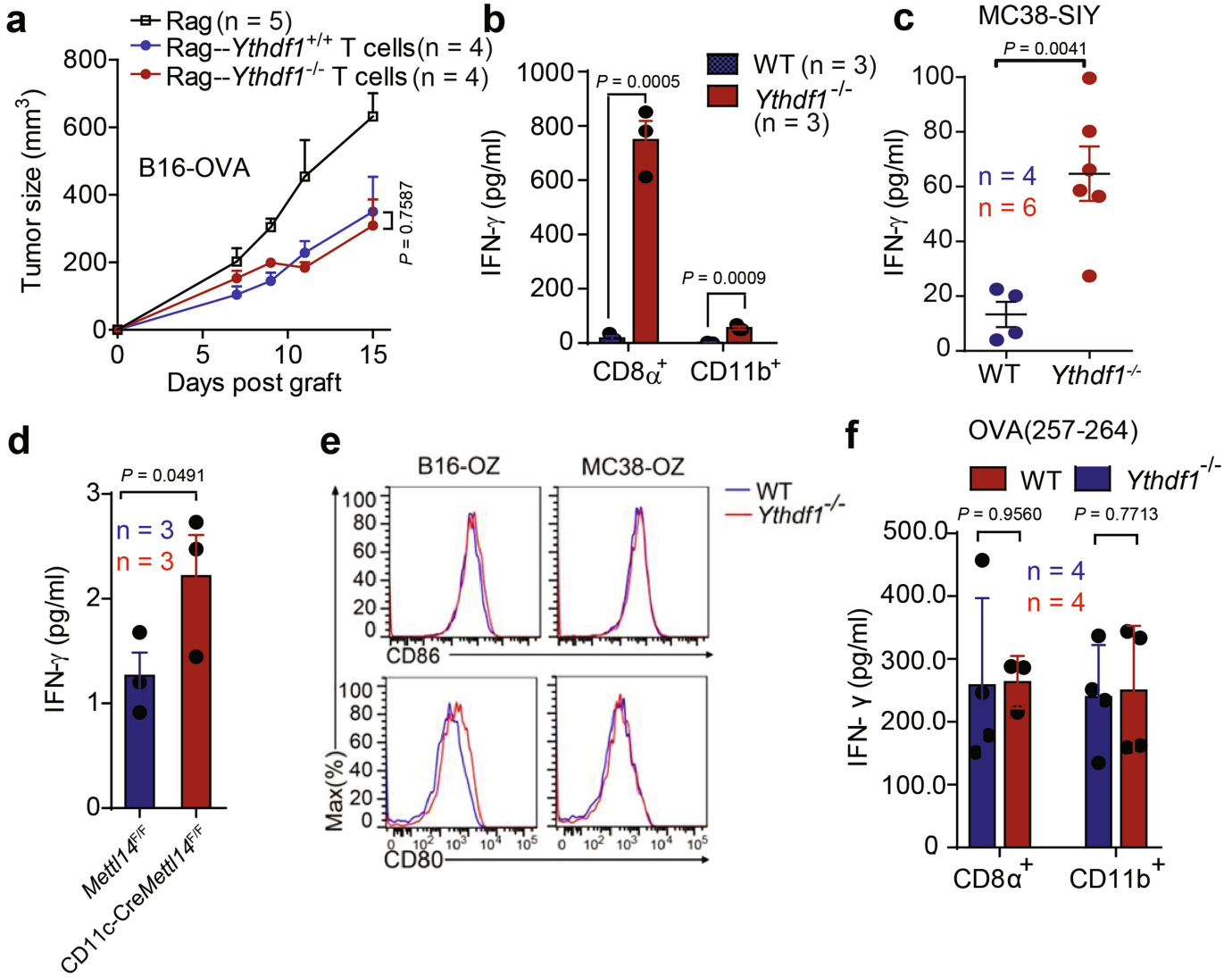

Extended Data Fig. 3 | Cross-priming of tumour neoantigens is increased in *Ythdf1*$^{-/-}$ mice. a, *Rag2*$^{-/-}$ mice were inoculated with T cells isolated from wild-type or *Ythdf1*$^{-/-}$ mice on day 0. On the same day, mice were injected s.c. with 5×10^5 B16-OVA cells. Tumour growth was monitored over time. **b**, Wild-type or *Ythdf1*$^{-/-}$ mice were injected s.c. with 10^6 MC38-OTIp cells. Six days after tumour inoculation, CD8$^+$ or CD11b$^+$ DCs were sorted from DLNs. DCs were co-cultured with CD8$^+$ T cells isolated from naive OT-I mice. Cross-priming capacity was determined by the production of IFNγ. **c**, Wild-type or *Ythdf1*$^{-/-}$ mice were injected s.c. with 10^6 MC38-SIY cells. Six days after tumour inoculation, DCs were sorted from DLNs and co-cultured with CD8$^+$ T cells isolated from naive 2C mice. Cross-priming capacity was determined by the production of IFNγ. **d**, Wild-type or *Mett14*-deficient GMDCs were co-cultured with B16-OVA cells. Cross-priming capacity was determined by the production of IFNγ. **e**, Wild-type and *Ythdf1*$^{-/-}$ mice were injected s.c. with 10^6 B16-OVA cells. Data are shown as the expression of CD80 and CD86 on tumour-infiltrating DCs. **f**, Wild-type and *Ythdf1*$^{-/-}$ mice were injected s.c. with 10^6 B16-OVA cells. Six days after tumour inoculation, CD8$^+$ or CD11b$^+$ DCs were sorted from DLNs. DCs were pulsed with 1 μg/ml exogenous OT-I peptide and co-cultured with isolated CD8$^+$ T cells from naive OT-I mice for 3 days, and then analysed by IFNγ CBA. Data are representative of two independent experiments with similar results (**e**). *n*, number of mice. Mean ± s.e.m., two-sided unpaired Student's *t*-test (**a**–**c**, **f**) or one-sided unpaired Student's *t*-test (**d**).

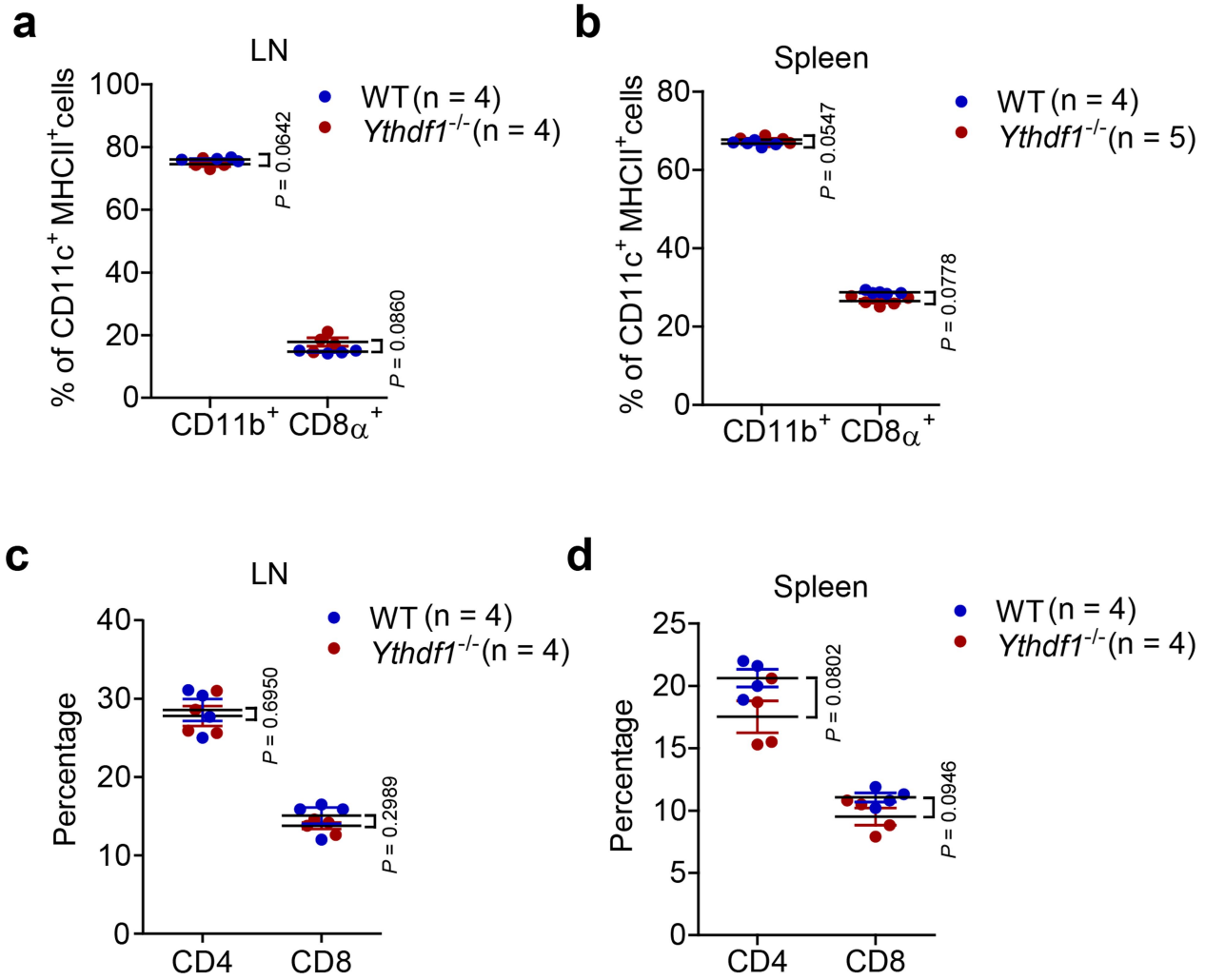

Extended Data Fig. 4 | Development of DCs and T cells is similar in *Ythdf1*$^{+/+}$ and *Ythdf1*$^{-/-}$ mice. a, **b**, Percentages of CD11b^{+} and CD8α^{+} DCs in lymph node (LN) and spleen. **c**, **d**, Percentages of CD4^{+} and CD8^{+} T cells in lymph node and spleen. No significant difference was detected between wild-type and *Ythdf1*$^{-/-}$ mice. *n*, number of mice. Mean ± s.e.m., two-sided unpaired Student's *t*-test.

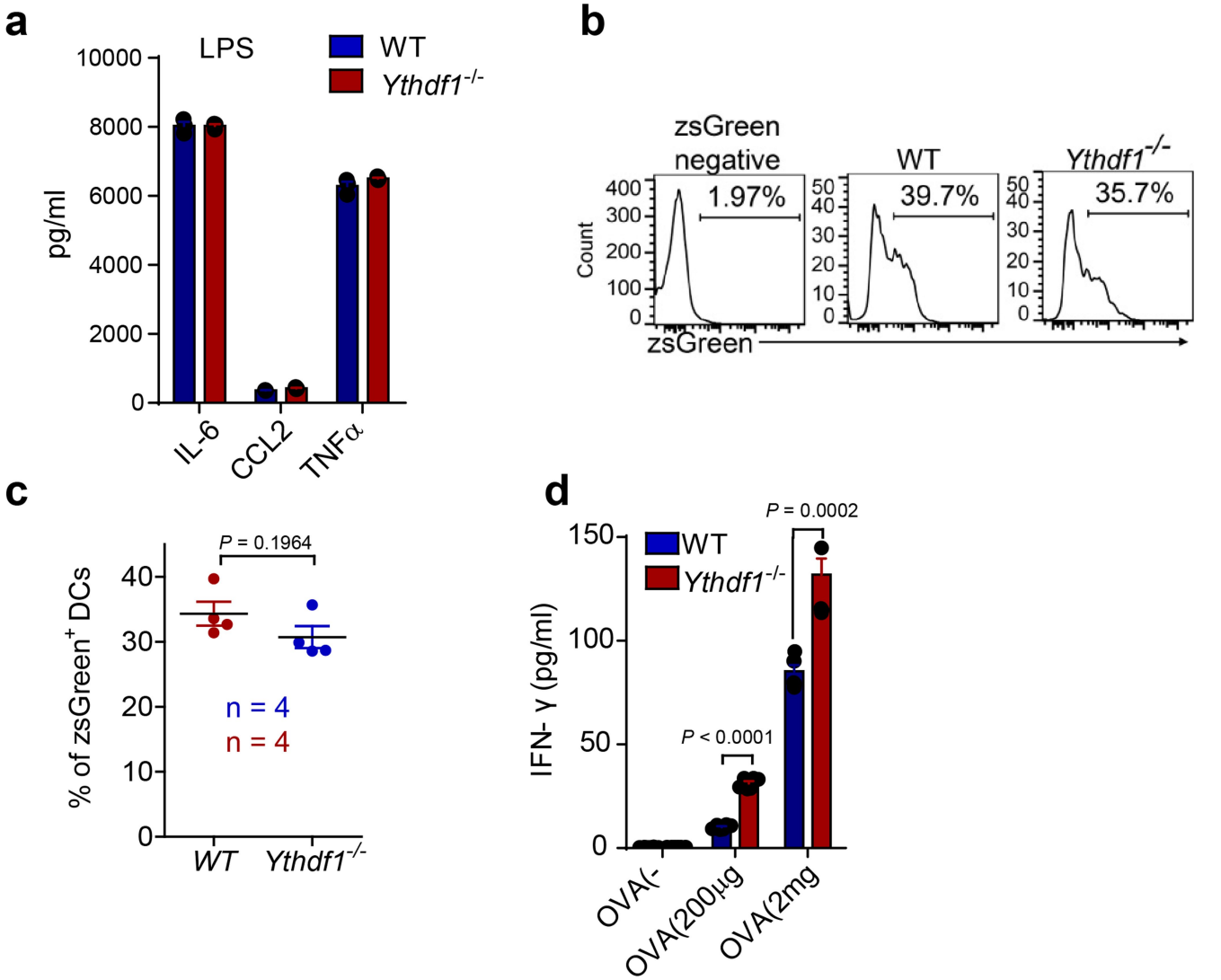

Extended Data Fig. 5 | In vitro functional analysis of GMDCs generated from *Ythdf1*$^{-/-}$ mice. a, Production of IL-6, CCL2 and TNFα upon stimulation of *Ythdf1*$^{-/-}$ GMDCs with LPS. **b**, **c**, Wild-type and *Ythdf1*$^{-/-}$ mice were injected s.c. with 10^6 B16-OTI-zsGreen cells. The percentage of tumour-infiltrating zsGreen$^+$ DCs six days after tumour inoculation is shown. Data are representative of two independent experiments (**b**). **d**, Splenic DCs from wild-type and *Ythdf1*$^{-/-}$ mice were stimulated with LPS overnight. The cross-presentation capacity of DCs in response to soluble OVA was assessed. $n = 3$ independent experiments (**a**); $n = 6$ independent experiments (**d**). *n*, number of mice. Mean ± s.e.m., two-sided unpaired Student's *t*-test.

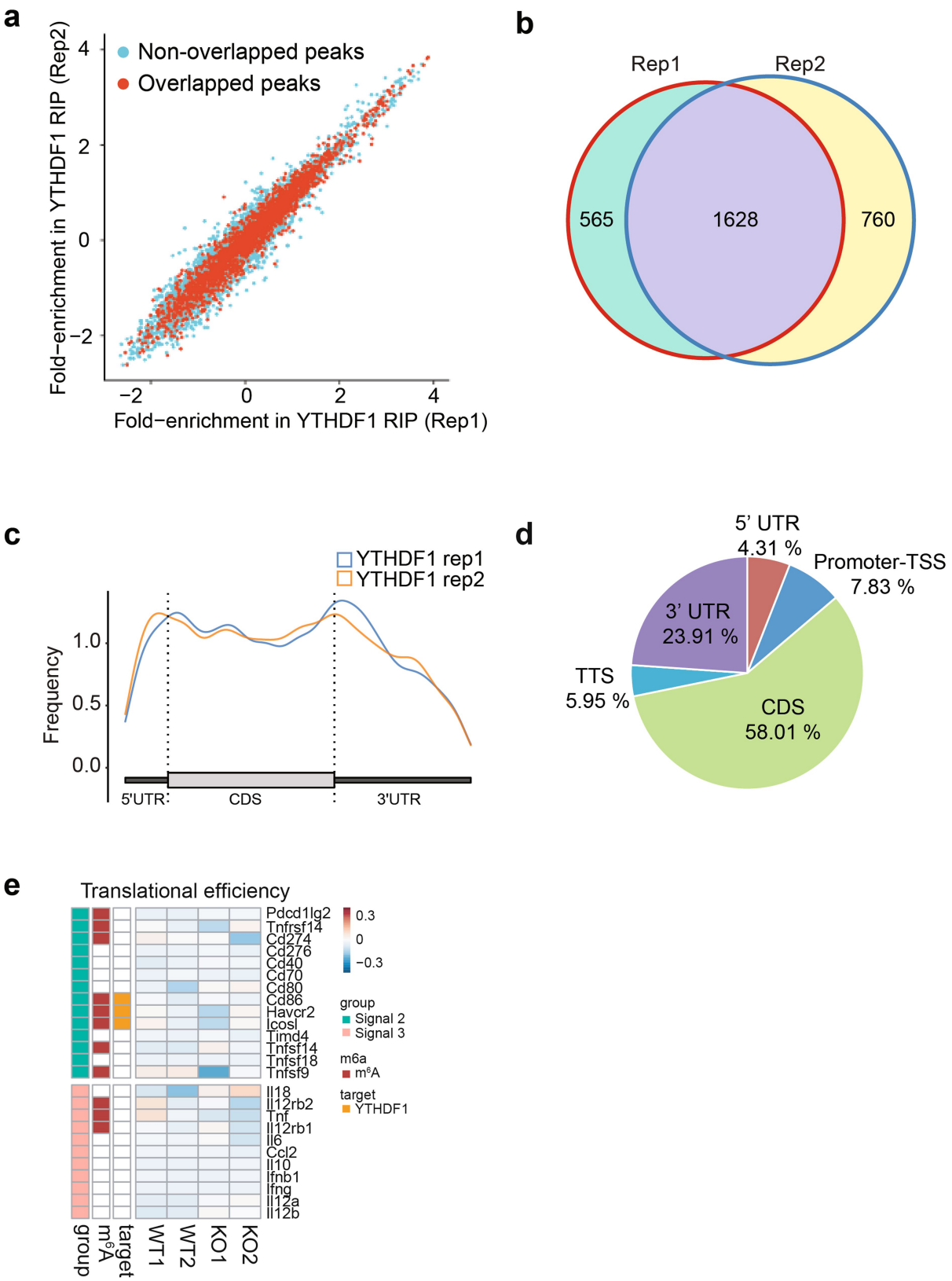

Extended Data Fig. 6 | Transcriptome-wide analysis of YTHDF1-binding sites in FLT3L-DCs. a, High reproducibility of YTHDF1 RIP–seq data. For each potential YTHDF1 binding peak, the fold-enrichment of the RIP/input signal was determined for both replicate 1 (Rep1) and replicate 2. Peaks identified in both replicates were considered as high-confidence peaks and are indicated in red. **b**, Overlap of YTHDF1-binding transcripts revealed from RIP–seq of two biological replicates. **c**, Meta-gene analysis to show the distribution of YTHDF1-binding sites along a normalized transcript. **d**, Distribution of YTHDF1-binding sites in transcripts. TTS, transcription termination site. **e**, Heatmap showing the translational efficiency of co-simulatory/inhibitory proteins (signal 2) and cytokines (signal 3) in wild-type and *Ythdf1*$^{-/-}$ FLT3L-DCs.

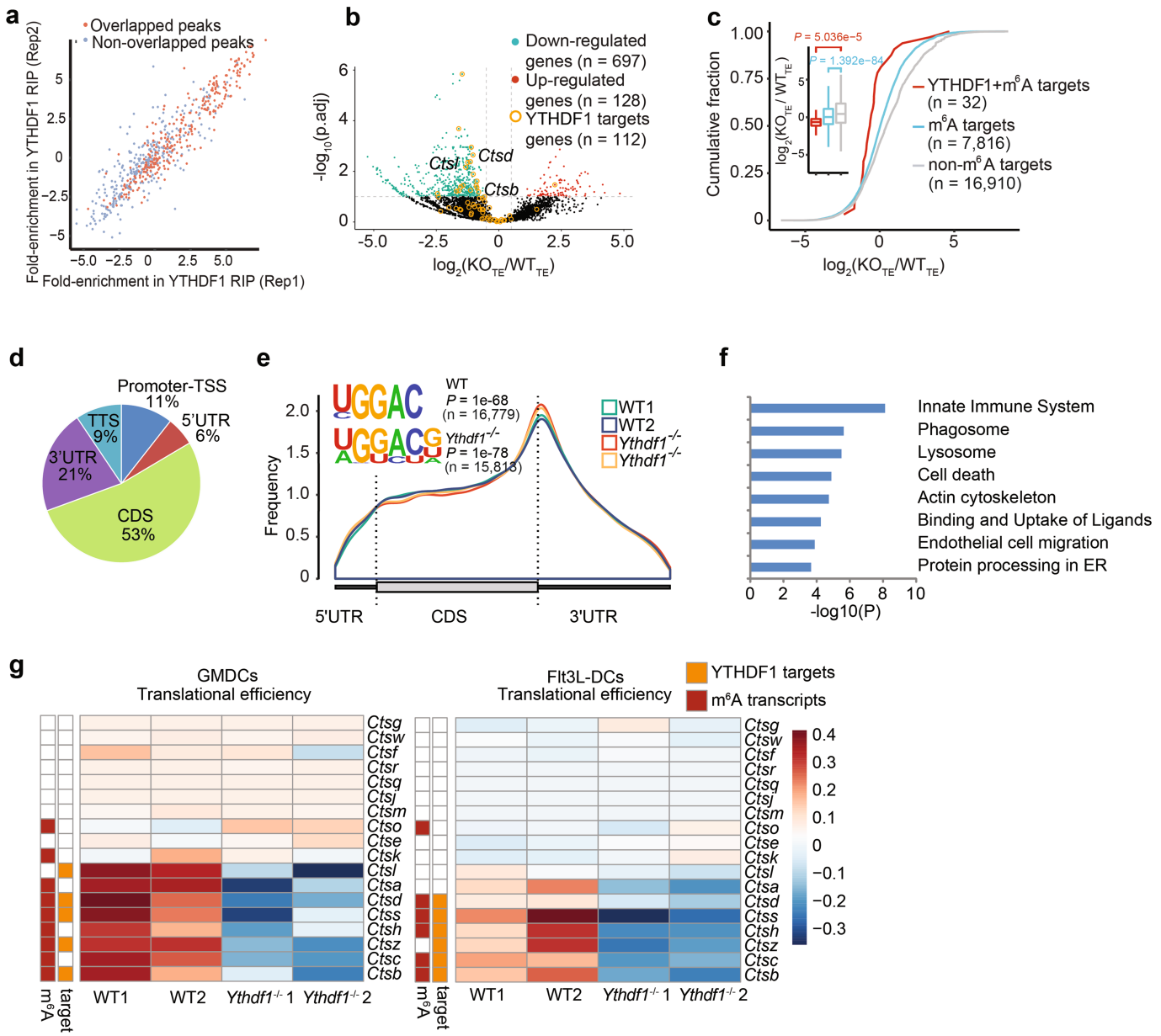

Extended Data Fig. 7 | THDF1-deficient GMDCs exhibit lower translational rates. a, High reproducibility of YTHDF1 RIP-seq data in GMDCs. For each potential YTHDF1 binding peak, the fold-enrichment of the RIP/input signal was determined for both Replicate 1 and Replicate 2. Peaks identified in both replicates were considered high-confidence peaks and are indicated in red. **b**, Volcano plots of genes with differential translational efficiencies in wild-type and *Ythdf1*$^{-/-}$ GMDCs. YTHDF1 targets are marked with yellow circles. *P* values calculated using two-sided likelihood ratio test with Benjamini–Hochberg adjustment; $n = 4$ (2 conditions × 2 biological replicates). **c**, Cumulative distribution of the fold change in translational efficiency between wild-type and *Ythdf1*$^{-/-}$ GMDCs. *P* values calculated using two-sided Kolmogorov–Smirnov test; $n = 2$ independent biological replicates. Box-plot elements: centre line, median; box limits, upper and lower quartiles; whiskers, 1–99%. **d**, Distribution of YTHDF1-binding sites in transcripts. **e**, Metagene plot depicting nearly unchanged distribution of m^{6}A peaks and similar consensus motifs in wild-type and *Ythdf1*$^{-/-}$ GMDCs. *P* values of consensus motifs generated by HOMER[29] using one-sided binomial test. **f**, KEGG and GO enrichment analysis of YTHDF1 target genes revealed enrichment of biological functions related to the innate immune system, lysosomes and phagosomes ($n = 79$). One-sided hypergeometric test was used to determine the statistical significance of enrichment. **g**, Heatmap showing translational efficiency of cathepsin genes in GMDCs and FLT3L-DCs. *n*, number of genes or m^{6}A peaks.

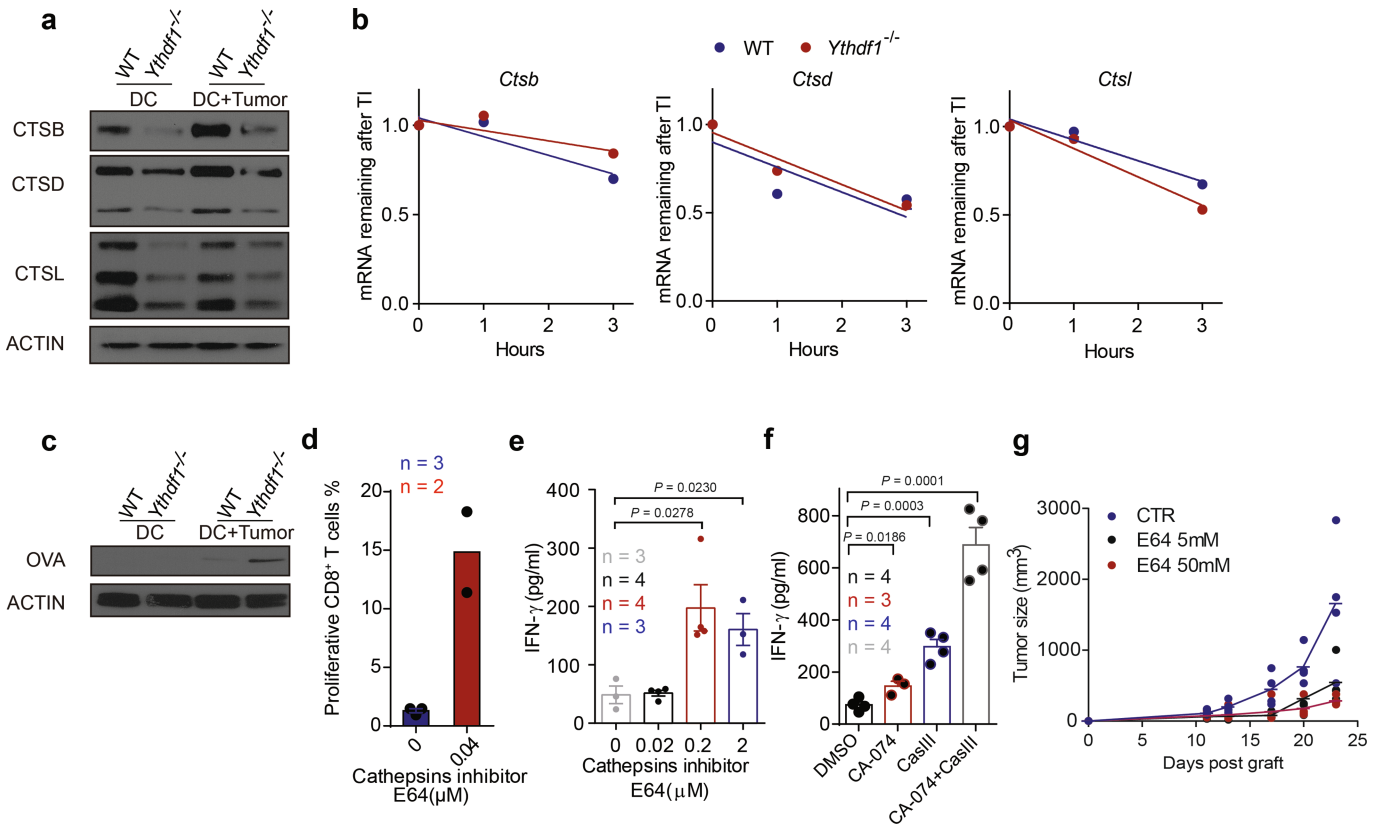

Extended Data Fig. 8 | Antigen degradation is reduced in *Ythdf1*$^{-/-}$ mice and inhibition of protease cathepsins enhances cross-priming of wild-type DCs. a, GMDCs were co-cultured with necrotic B16-OVA cells overnight. Immunoblot analysis of cathespins B, D and L (CTSB, CTSD and CTSL) in GMDCs. **b**, Wild-type and *Ythdf1*$^{-/-}$ DCs were treated with actinomycin D and RNAs were collected at different time points after treatment. mRNA levels were measured using RT–qPCR and represented as mRNA remaining after transcription inhibition (TI). **c**, GMDCs were co-cultured with necrotic B16-OVA cells overnight and OVA degradation in BMDCs was measured by immunoblot. **d**, Ex vivo purified wild-type cDCs were pre-treated with 0.04 μM E64 and pulsed with OVA protein for 4 h. The cross-priming capacity of DCs was compared by co-culturing DCs with CTV-labelled OT-I T cells. Proliferation was measured by the dilution of CTV. **e**, GMDCs were pre-treated with 0.2–2 μM E64 and co-cultured with B16-OVA cells. The cross-priming capacity of DCs was compared by co-culturing DCs with isolated CD8$^+$ T cells from naive OT-I mice and analysed by IFNγ CBA. **f**, FLT3L-DCs were pre-treated with cathepsin inhibitor CA-074 or/and cathepsin L inhibitor III (CASIII), followed by co-culturing with necrotic B16-OVA cells. Synergistic inhibition was observed. The cross-priming capacity of DCs was determined. **g**, Data points for Fig. 4b. $n = 3$ independent experiments with similar results (**a**, **c**); $n = 2$ independent experiments (**b**). *n*, sample size. Mean ± s.e.m., two-sided unpaired Student's *t*-test (**e**) or one-sided unpaired Student's *t*-test (**f**).

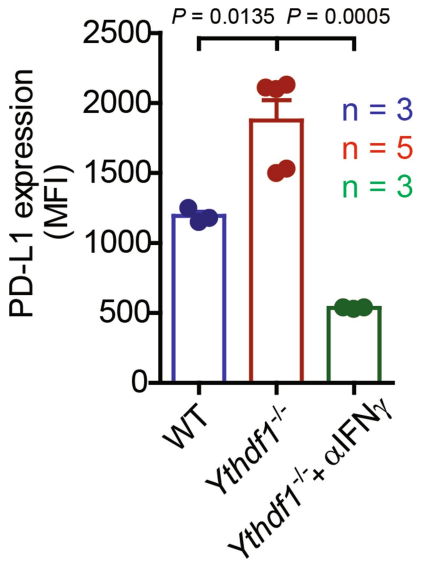

Extended Data Fig. 9 | IFNγ in tumour tissues is responsible for the upregulation of PD-L1 in *Ythdf1*$^{-/-}$ mice. Tumour-bearing mice were treated with 50 μg anti-IFNγ monoclonal antibody intratumorally and PD-L1 expression on tumour cells is shown. *n*, number of mice. Mean ± s.e.m., two-sided unpaired Student's *t*-test.

nature research

Corresponding author(s): Chuan He

Last updated by author(s): Jan 1, 2019

Reporting Summary

Nature Research wishes to improve the reproducibility of the work that we publish. This form provides structure for consistency and transparency in reporting. For further information on Nature Research policies, see Authors & Referees and the Editorial Policy Checklist.

Statistics

For all statistical analyses, confirm that the following items are present in the figure legend, table legend, main text, or Methods section.

n/a	Confirmed	
☐	☒	The exact sample size (*n*) for each experimental group/condition, given as a discrete number and unit of measurement
☐	☒	A statement on whether measurements were taken from distinct samples or whether the same sample was measured repeatedly
☐	☒	The statistical test(s) used AND whether they are one- or two-sided *Only common tests should be described solely by name; describe more complex techniques in the Methods section.*
☒	☐	A description of all covariates tested
☐	☒	A description of any assumptions or corrections, such as tests of normality and adjustment for multiple comparisons
☐	☒	A full description of the statistical parameters including central tendency (e.g. means) or other basic estimates (e.g. regression coefficient) AND variation (e.g. standard deviation) or associated estimates of uncertainty (e.g. confidence intervals)
☐	☒	For null hypothesis testing, the test statistic (e.g. *F*, *t*, *r*) with confidence intervals, effect sizes, degrees of freedom and *P* value noted *Give P values as exact values whenever suitable.*
☒	☐	For Bayesian analysis, information on the choice of priors and Markov chain Monte Carlo settings
☒	☐	For hierarchical and complex designs, identification of the appropriate level for tests and full reporting of outcomes
☐	☒	Estimates of effect sizes (e.g. Cohen's *d*, Pearson's *r*), indicating how they were calculated

Our web collection on statistics for biologists contains articles on many of the points above.

Software and code

Policy information about availability of computer code

Data collection	Cell images were collected with with a Nikon Eclipse Ti2 with NIS Elements Imaging Software (Version 5.02).
Data analysis	Images analyzed with ImageJ (Version 1.52e). Experimental data were analyzed using Prism 5.0 software (GraphPad). For sequencing data, reads were post-processed and aligned to the mouse mm9 assembly using STAR program (version 2.6.0c). To visualize sequencing signals in the genome browser, we generated bigwig files with bamCoverage function from deepTools (version 3.0.1). For RIP-Seq, Piranha (version 1.2.1) software was to detect the binding sites of YTHDF1. For m6A-Seq, the m6A-enriched regions (peaks) in each m6AIP samples were detected by MACS2 (version 2.1.1.20160309). Metagene plots were performed by the Bioconductor GUITAR package (version 1.16.0). Peaks that were detected by both replicates were considered as high confident peaks. GO term analyses were performed by metascape. For Ribo-seq, adapter sequences were firstly trimmed from sequencing reads by using fastx_trimmer (version 0.0.14) and cutadapt (version 1.15). Trimmed reads were filtered for mitochondrial DNA and ribosomal RNA by Bowtie2 (version 2.3.4). Uniquely mapped reads were selected by using SAMtools (version 1.7). The raw counts of coding regions were calculated by HOMER (version 4.9). The differentially translational efficiency genes were detected by Bioconductor DESeq2 package (Version 1.18.1). The flow cytometry data were analyzed by Flowjo 7.0 (Treestar).

For manuscripts utilizing custom algorithms or software that are central to the research but not yet described in published literature, software must be made available to editors/reviewers. We strongly encourage code deposition in a community repository (e.g. GitHub). See the Nature Research guidelines for submitting code & software for further information.

Data

Policy information about availability of data

All manuscripts must include a data availability statement. This statement should provide the following information, where applicable:

- Accession codes, unique identifiers, or web links for publicly available datasets
- A list of figures that have associated raw data
- A description of any restrictions on data availability

Ribo-seq, RIP-seq and m6A-seq data generated by this study have been deposited in the GEO database under the accession number GSE115106. A summary of the sequencing experiment can be found in Supplementary Table 3. The differential translational efficiency results provided in Supplementary Table 4. All other data supporting the findings of this study are available from the corresponding author on reasonable request.

Field-specific reporting

Please select the one below that is the best fit for your research. If you are not sure, read the appropriate sections before making your selection.

☒ Life sciences ☐ Behavioural & social sciences ☐ Ecological, evolutionary & environmental sciences

For a reference copy of the document with all sections, see nature.com/documents/nr-reporting-summary-flat.pdf

Life sciences study design

All studies must disclose on these points even when the disclosure is negative.

Sample size	In general, no statistical methods were used to predetermine sample size. For the animal experiments, sample size was determined based on our prior experience of performing similar sets of experiments and literature reports. For human samples, samples were collected till we have sufficient number to obtain statistically reliable estimates. For cell and biochemical data, we aimed to collect data from three or more biological replicates when possible.
Data exclusions	No data were excluded from the analysis
Replication	Experiments were independently repeated two to three times. All attempt to reproduce the results were successful.
Randomization	Mice were assigned at random to treatment groups for all mouse studies and, where possible, mixed among cages.
Blinding	Reported in the 'Statistical analysis and reproducibility' section of the Methods. For IHC experiment, blinded staining and blinded analysis were performed. For other experiments, the investigators were not blinded to the group allocation, as group allocation was clearly visible in the samples due to phenotypic changes. Variations were controlled through replicates.

Reporting for specific materials, systems and methods

We require information from authors about some types of materials, experimental systems and methods used in many studies. Here, indicate whether each material, system or method listed is relevant to your study. If you are not sure if a list item applies to your research, read the appropriate section before selecting a response.

Materials & experimental systems

n/a	Involved in the study
☐	☒ Antibodies
☐	☒ Eukaryotic cell lines
☒	☐ Palaeontology
☐	☒ Animals and other organisms
☐	☒ Human research participants
☒	☐ Clinical data

Methods

n/a	Involved in the study
☒	☐ ChIP-seq
☐	☒ Flow cytometry
☒	☐ MRI-based neuroimaging

Antibodies

Antibodies used	Goat HRP-anti-GAPDH WB 1:10000 ProteinTech HRP-60004 Rabbit anti-YTHDF1 IP&WB 1:100 for IP, 1:1000 for WB ProteinTech 17479-1-AP Rabbit anti-YTHDF2 WB 1:1000 ProteinTech 24744-1-AP Anti-rabbit IgG-HRP WB 1:5000 cell signaling technology 7074S Mouse anti-YTHDF3 WB 1:500 Santa-Cruz sc-377119 F-2 Anti-mouse IgG-HRP WB 1:5000 cell signaling technology 7076S Rabbit anti-YTHDC1 WB 1:1000 Abcam ab122340

Goat anti-YTHDC2 WB 1:500 Santa-Cruz sc-249370 G-19
Anti-goat IgG-HRP WB 1:5000 Abcam ab6741
Anti-Chicken Egg Albumin antibody produced in rabbit WB 1:5000 Sigma C6534-2ML
Mouse/Rat Cathepsin L Antibody WB 1:1000 R&D AF1515
β-Actin Antibody (C4) HRP WB 1:2000 Santa-Cruz sc-47778 HRP
InVivoMAb anti-mouse CD16/CD32 FcγR blockade 1:500 BioX Cell BE0307 2.4G2
CD11c Monoclonal Antibody (N418), PE-Cyanine7 Flow cytometry 1:500 eBioscience 25-0114-82 N418
PerCP/Cy5.5 Anti-Mouse/Human CD11b Flow cytometry 1:500 Biolegend 101228 M1/70
FITC Anti-Mouse Ly-6C Flow cytometry 1:500 Biolegend 128005 HK1.4
Brilliant Violet 510™ anti-mouse I-A/I-E Flow cytometry 1:500 Biolegend 107635 M5/114.15.2
AF 647 Anti-Mouse F4/80 Flow cytometry 1:500 eBioscience 132121 BM8
APC/Cy7 Anti-Mouse CD45 Flow cytometry 1:500 Biolegend 103116 30-F11
Brilliant Violet 510™ anti-mouse CD24 Flow cytometry 1:500 Biolegend 101831 M1/69
PE Hamster Anti-Mouse CD80 Flow cytometry 1:500 BD Biosciences 553769 16-10A1
PE/Cy5 Anti-Mouse CD86 Flow cytometry 1:500 Biolegend 105016 GL-1
PE anti-mouse CD274 (B7-H1, PD-L1) Flow cytometry 1:500 Biolegend 124308 10F.9G2
PE-Cy7 Anti-Mouse CD4 Flow cytometry 1:500 eBioscience 25-0041-82 GK1.5
PE Anti-Mouse CD8a Flow cytometry 1:500 Biolegend 100708 53-6.7
PE anti-mouse CD107a (LAMP-1) Flow cytometry 1:500 Biolegend 121612 1D4B
FITC Anti-Mouse CD25 Flow cytometry 1:500 Biolegend 101907 3C7
FITC anti-mouse/human CD45R/B220 Flow cytometry 1:501 Biolegend 103206 RA3-6B2
PE anti-mouse/rat/human FOXP3 Flow cytometry 1:500 Biolegend 320008 150D
OVA257-264 (SIINFEKL) peptide bound to H-2Kb Monoclonal Antibody Flow cytometry 1:500 Thermofisher 12-5743-82 25-D1.16
NK1.1 Monoclonal Antibody (PK-136), Pacific Blue Flow cytometry 1:500 Thermofisher MM6628 PK136
iTAg Tetramer/PE - H-2 Kb OVA (SIINFEKL) Flow cytometry 1:500 MBL TB-5001-1
Cathepsin A Rabbit polyAb Flow cytometry 1:200 Proteintech 15020-1-AP
Cathepsin H Rabbit polyAb Flow cytometry 1:200 Proteintech 10315-1-AP
Cathepsin B (D1C7Y) Rabbit mAb Flow cytometry & WB 1:300 for flow cytometry, 1: 1000 for WB cell signaling technology 31718S D1C7Y
Rb mAb to Cathepsin D Flow cytometry & WB 1:300 for flow cytometry, 1: 1000 for WB Abcam ab75852 EPR3057Y
Alexa Fluor 568 Goat-anti-Rabbit IgG Flow cytometry 1:500 ThermoFisher A-11036
InVivoMAb anti-mouse NK1.1 In vivo depletion 200μg BioX Cell BE0036 PK136
InVivoMAb anti-mouse CD8α In vivo depletion 200μg BioX Cell BE0117 YTS169.4
InVivoMAb anti-mouse IFNγ In vivo blockade 50μg BioX Cell BE0055 XMG1.2
anti-IFNγ antibody ELISPOT 1:250 BD Biosciences 554408 XMG1.3
CD8 IHC 1:400 DAKO M7103 C8/144B

Validation

All the primary antibodies we used were validated by manufacturers

Eukaryotic cell lines

Policy information about cell lines

Cell line source(s)

MC38 cell lines were provided by D. Bartlett (University of Pittsburgh, Pittsburgh, PA). B16-OVA cells were provided by Dr. Yang-Xin Fu (UT Southwestern). B16F10 cell line was purchased from ATCC.

Authentication

All cell lines were authenticated according the ATCC cell line authentication test recommendations that included a morphology check by microscope, growth curve analysis and mycoplasma check.

Mycoplasma contamination

All cell lines are mycoplasma-free.

Commonly misidentified lines
(See ICLAC register)

No cell line listed by ICLAC was used.

Animals and other organisms

Policy information about studies involving animals; ARRIVE guidelines recommended for reporting animal research

Laboratory animals

Female Rag2-/- mice, 2C CD8+ T cell receptor (TCR)-Tg, CD11c-Cre and Zbtb46-DTR mice were purchased from Jackson laboratory. Female Ythdf1-/- mice and CD11c-CreMettl14f/f conditional knockout mice were generated in house. All mice were used at 6–12 weeks of age. All the mice were maintained under specific pathogen-free conditions and used in accordance with the animal experimental guidelines set by the Institute of Animal Care and Use Committee.

Wild animals

The study did not involve wild animals.

Field-collected samples

The study did not involve filed-collected samples.

Ethics oversight

All animal procedures used in this experiment were performed in accordance with protocols approved by the Institutional Animal Care and Use Committee of University of Chicago.

Note that full information on the approval of the study protocol must also be provided in the manuscript.

Human research participants

Policy information about studies involving human research participants

Population characteristics	Information about the patient sex, age, and tumor characteristics are given in Supplementary Table 2. 9 female and 13 male patients with age ranging from 42.1-86.8 and presented with adenocacinoma colon cancer at various stages and locations were studied. Controlling for covariates was not necessary as the analyses correlate CD8 and YTHDF1 in stroma taken from the same patient.
Recruitment	Participants were recruited from the pool of patients at the University of Chicago. There may be self selection biases based on individuals who are able to seek care at the institution. The sample should be representative of the populations served by the institution.
Ethics oversight	All samples were obtained with informed consent under a protocol approved by the University of Chicago Institutional Review Board.

Note that full information on the approval of the study protocol must also be provided in the manuscript.

Flow Cytometry

Plots

Confirm that:

☒ The axis labels state the marker and fluorochrome used (e.g. CD4-FITC).

☒ The axis scales are clearly visible. Include numbers along axes only for bottom left plot of group (a 'group' is an analysis of identical markers).

☒ All plots are contour plots with outliers or pseudocolor plots.

☒ A numerical value for number of cells or percentage (with statistics) is provided.

Methodology

Sample preparation	For flow cytometric analysis and cell sorting, tumors, lymph nodes and spleens were collected from mice and digested with 0.26U/ml Liberase TM and 0.25mg/ml DNase I at 37°C for 30min. Samples were then filtered through a 70µm cell strainer and washed twice with staining buffer. Cells were re-suspended in staining buffer (PBS with 2% FCS and 0.5 M EDTA).
Instrument	Cells were either analyzed on a BD Fortessa (BD) or sorted by AriaIIIu (BD).
Software	Analysis of flow cytometry data was performed using Flowjo 7.0 (Treestar).
Cell population abundance	The purity of sorted cells was detected via Fortessa and samples with purity >90% were used.
Gating strategy	cell populations were determined by A FSC-H/FSC-A gate. The boundaries were determined by the clear cell subpopulations and isotype controls.

☐ Tick this box to confirm that a figure exemplifying the gating strategy is provided in the Supplementary Information.